Evaluation of Dynamical Downscaling in a Fully Coupled Regional Earth System Model

Mark W. Seefeldt[1], John J. Cassano[1], Younjoo J Lee[2], Wieslaw Maslowski[2], Anthony Craig[2], and Robert Osinski[3]

[1]University of Colorado Boulder
[2]Naval Postgraduate School
[3]Institute of Oceanology of Polish Academy of Sciences

January 24, 2023

Abstract

A set of decadal simulations has been completed and evaluated for gains using the Regional Arctic System Model (RASM) to dynamically downscale data from a global Earth system model (ESM) and two atmospheric reanalyses. RASM is a fully coupled atmosphere - land - ocean - sea ice regional Earth system model. Nudging to the forcing data is applied to approximately the top half of the atmosphere. RASM simulations were also completed with a modification to the atmospheric physics for evaluating changes to the modeling system. The results show that for the top half of the atmosphere, the RASM simulations follow closely to that of the forcing data, regardless of the forcing data. The results for the lower half of the atmosphere, as well as the surface, show a clustering of atmospheric state and surface fluxes based on the modeling system. At all levels of the atmosphere the imprint of the weather from the forcing data is present as indicated in the pattern of the monthly and annual means. Biases, in comparison to reanalyses, are evident in the ESM forced simulations for the top half of the atmosphere but are not present in the lower atmosphere. This suggests that bias correction is not needed for fully-coupled dynamical downscaling simulations. While the RASM simulations tended to go to the same mean state for the lower atmosphere, there is a different evolution of the weather across the ensemble of simulations. These differences in the weather result in variances in the sea ice and oceanic states.

Hosted file

953355_0_art_1_rtkhth.docx available at https://authorea.com/users/578040/articles/620178-evaluation-of-dynamical-downscaling-in-a-fully-coupled-regional-earth-system-model

Hosted file

953355_0_figure_10620291_r4qsr3.docx available at https://authorea.com/users/578040/articles/620178-evaluation-of-dynamical-downscaling-in-a-fully-coupled-regional-earth-system-model

Hosted file

953355_0_supp_10580738_rnwhtf.docx available at https://authorea.com/users/578040/articles/620178-evaluation-of-dynamical-downscaling-in-a-fully-coupled-regional-earth-system-model

Evaluation of Dynamical Downscaling in a Fully Coupled Regional Earth System Model

Mark W. Seefeldt[1], John J. Cassano[1,2], Younjoo J. Lee[3], Wieslaw Maslowski[3], Anthony P. Craig[4], and Robert Osinski[5]

[1]National Snow Ice and Data Center, Cooperative Institute for Research in Environmental Sciences, University of Colorado Boulder, Boulder, CO, USA

[2]Department of Atmospheric and Oceanic Sciences, University of Colorado Boulder, Boulder, CO, USA

[3]Department of Oceanography, Naval Postgraduate School, Monterey, CA, USA

[4]Independent Researcher

[5]Institute of Oceanology, Polish Academy of Sciences, Sopot, Poland

Corresponding author: Mark W. Seefeldt (mark.seefeldt@colorado.edu)

Key Points:

- The near-surface and lower atmosphere mean climatic state are clustered together based on the modeling system more so than the forcing data.
- Bias correction of Earth system model data is not necessary for dynamical downscaling using a fully coupled regional Earth system model.
- There are variances in sea ice and oceanic states despite the simulations having similar climatic states for the lower atmosphere.

Abstract

A set of decadal simulations has been completed and evaluated for gains using the Regional Arctic System Model (RASM) to dynamically downscale data from a global Earth system model (ESM) and two atmospheric reanalyses. RASM is a fully coupled atmosphere – land – ocean – sea ice regional Earth system model. Nudging to the forcing data is applied to approximately the top half of the atmosphere. RASM simulations were also completed with a modification to the atmospheric physics for evaluating changes to the modeling system. The results show that for the top half of the atmosphere, the RASM simulations follow closely to that of the forcing data, regardless of the forcing data. The results for the lower half of the atmosphere, as well as the surface, show a clustering of atmospheric state and surface fluxes based on the modeling system. At all levels of the atmosphere the imprint of the weather from the forcing data is present as indicated in the pattern of the monthly and annual means. Biases, in comparison to reanalyses, are evident in the ESM forced simulations for the top half of the atmosphere but are not present in the lower atmosphere. This suggests that bias correction is not needed for fully-coupled dynamical downscaling simulations. While the RASM simulations tended to go to the same mean state for the lower atmosphere, there is a different evolution of the weather across the ensemble of simulations. These differences in the weather result in variances in the sea ice and oceanic states.

Plain Language Summary

Regional Earth system models are used to provide added value to numerical simulations of the climate system by using the output data from global Earth system model(s), or reanalyses, to force the simulations. The Regional Arctic System Model (RASM) is a fully coupled atmosphere – land – ocean – sea ice regional Earth system model. This study uses RASM to dynamically downscale data from an ensemble of simulations from an Earth system model and two reanalyses to evaluate the gains and characteristics in dynamical downscaling with a fully coupled regional model. The results indicate the near-surface and lower atmosphere mean climatic state are clustered together based on the modeling system more so than the forcing data. Meanwhile the ensemble of simulations resulted in variances in sea ice and oceanic states despite the simulations having similar climatic states for the lower atmosphere. The differences in sea ice and oceanic states in the fully coupled regional model are the result of differences in weather, or the sequencing of atmospheric circulation patterns, in the forcing conditions.

1 Introduction

Regional climate models (RCMs) have been developed and implemented to bridge the gap between the large-scale Earth system models (ESMs) and for providing an understanding of regional concerns, impacts, and physical processes (Giorgi, 2019; Gutowski et al., 2020). This regional modeling is also commonly referred to as dynamical downscaling as it is downscaling the output from the coarser resolution of the ESM to that of a higher resolution applied to a region of interest. Dynamical downscaling applies the equations representing the physics and dynamics of the atmosphere at a higher spatial resolution than that of the forcing dataset. An ESM, or a reanalysis of the atmosphere, provides the forcing dataset for the initial, lateral boundary, and if used, nudging conditions for the downscaled simulations. RCMs have the benefit of representing complex interactions with local topography, interactions between regional and local scale processes, optimizing the parameterizations for the physical processes of the selected region, and being computationally less expensive than ESMs.

RCMs are limited area models that are provided initial atmospheric conditions, as well as updated lateral boundary conditions, as the RCM is integrated forward in time. However, the interior of the domain tends to drift to anomalous behavior as it goes away from the prescribed lateral boundary conditions. This is especially true for RCMs employing large domains and integrated over climatic time scales. The concept of interior nudging was introduced to dampen the interior of the RCM domain toward the external forcing dataset and to get around this issue of drift. The goal in applying nudging is to maintain the large-scale features of the forcing data but to simultaneously allow for the small-scale features to evolve based on the RCM. One way to achieve this goal is to apply the nudging to approximately the top half of the model domain. This allows for the RCM to be nudged towards the large-scale circulation features of the forcing data, while allowing the RCM to evolve in the bottom half of the model domain more freely. Bowden et al. (2012) compared three simulations: without nudging, with grid nudging, and with spectral nudging in the Weather Research and Forecasting (WRF) model. The grid nudging and spectral nudging were found to reduce the biases in comparisons to the simulations without nudging. Several other studies (e.g. Bullock et al., 2014; Cassano et al. 2011; Glisan et al., 2013; Liu et al., 2012) have collectively confirmed the benefits of either spectral or grid nudging with RCM simulations. In studies by Cassano et al. (2011) and Glisan et al. (2013) the nudging was used in WRF pan-Arctic simulations with the nudging applied to wind and temperature fields for the top half of the model domain, with a linearly ramping of nudging strength in a transition zone above the middle of the model domain.

Frequently, ESM data come with inherent biases in the output data because of imperfections in the modeling system, which can permeate into the RCM simulations. Bias correction is a method to reduce or eliminate such biases. A number of methods exist for applying a bias correction to the ESM data (Xu et al., 2021). Several studies have evaluated the application of bias corrected forcing data in RCM simulations (e.g. Hoffman et al., 2016; White and Toumi, 2013; Xu and Yang, 2015). In Bruyère et al. (2013) a mean bias correction method was applied to the ESM data. In this method the seasonal mean and perturbation terms are defined for the observations (reanalysis) and for the ESM, with the perturbation term defined for each six-hour interval. The bias corrected ESM data is the sum of the observations (reanalysis) seasonal mean and the ESM perturbation value for each six-hourly variable. Bruyère et al. (2013) indicate substantially improved results in comparison to observations for RCM simulations with bias correction applied than RCM simulations without bias correction.

Progress in recent years has been in the development and use of regional Earth system models (RESMs; Giorgi and Gao, 2018). RESMs include additional model components (e.g. lake, dynamic vegetation, biogeochemistry, sea ice and ocean models) in a coupled framework with the atmospheric model. Multi-component fully coupled models are becoming increasingly available, such as the Earth System Regional Climate model (RegCM-ES; Sitz et al., 2017) or the HIRHAM-NAOSIM (Yu et al., 2020). The Regional Arctic System Model (RASM; Cassano et al., 2017) is the multi-component, atmosphere-land-ocean-sea ice model used in this study. Overall, multi-component models involving the cryosphere, such as RASM, are key in understanding the climate projections in the polar regions because of the non-linear interactions between the cryosphere and other model components (Giorgi and Gao, 2018).

The goal for this study is to evaluate the atmospheric results from dynamical downscaling simulations using the fully coupled RASM, with an emphasis on the atmospheric state, circulation, and variability as well as their impact on sea ice and oceanic transports. The study focuses on three questions: i) does the use of nudging in the top half of the model limit the ability of RASM to develop its own near surface climate, ii) how does the downscaled RASM atmosphere respond to biases in the forcing data, and iii) what are the impacts of changes in the atmospheric forcing in a multi-component RESM on the coupled ocean and sea ice conditions? A key element of this dynamical downscaling study is that the surface state and fluxes are provided by the (active) coupled component models and not prescribed from the (passive) forcing datasets as is the case in an atmosphere-only dynamical downscaling. Section 2 covers the data sources and methods including a description of RASM, the ESM decadal ensemble, and the reanalyses used in the study, and a description of the experimental setup, including the configuration of RASM. Section 3 provides the results looking at monthly, annual, and multi-year means across the RASM model domain as well as for selected regions, followed by spatial analyses of the sea ice extent and temporal analyses of sea ice volume and oceanic volume transports across the main Arctic Ocean gateways. Section 4 provides a discussion of the results and conclusions.

2 Data Sources and Methods

2.1 Regional Arctic System Model

RASM (Cassano et al., 2017; Kinney et al., 2020; Hamman et al., 2016; Maslowski et al., 2012; Roberts et al, 2015) is a limited-area, fully coupled atmosphere-land-ocean-sea ice RESM with a focus on the Arctic. The RASM component models are the Weather Research and Forecasting (WRF v3.7.1, Powers et al., 2017) model for the atmosphere, the Variable Infiltration Capacity (VIC v4.0.6; Liang et al., 1994, 1996; modified as described in Hamman et al., 2016, Sec. 2b) model for the land hydrology and routing schemes (RVIC v1.0.0; Hamman et al., 2017), and regionally configured versions of the Parallel Ocean Program (POP v2.1; Smith et al., 2010) model for the ocean and the Los Alamos National Laboratory Sea Ice Model (CICE v6.0.0, Craig et al., 2018) for sea ice. The individual component models exchange fluxes and state values through the Community Earth System Model (CESM, Hurrell et al., 2013) coupler (CPL7, Craig et al., 2012). The CPL7 coupler has been modified for high spatiotemporal resolution coupling and for working with the individual component models (Roberts et al., 2015). RASM is run over a pan-Arctic domain (Figure 1) with the land and atmosphere sharing a polar-stereographic 50 km horizontal resolution domain with 40 vertical levels and a 50 hPa model top for the atmosphere, and three soil layers for the land. The ocean and sea ice share a 1/12° (~9 km) rotated sphere grid with a vertical resolution of 45 levels for POP and 5 thickness ice categories for CICE. There is an extended ocean region that covers the periphery of the ocean-sea ice domain to match the extent of the atmosphere-land domain (see Figure 1). This extended ocean domain uses climatological sea surface temperatures to provide the ocean-atmosphere fluxes, which are calculated in the coupler. More details of the broader RASM configuration and component models can be found in Roberts et al. (2015), Hamman et al. (2016), and Cassano et al. (2017).

A modified version of the Advanced Research WRF (WRF-ARW, hereafter simply WRF, Skamarock et al., 2008) model v3.7.1 is used as the atmospheric component in RASM.

The modifications to WRF address the coupling processes, exchange of fluxes, and the progression of WRF through model time in concert with the other component models. The CPL7 coupler exchanges surface fluxes and state variables from the land, ocean, and sea ice component models every 20 minutes of model time. The initial and lateral boundary conditions for WRF in RASM are provided by the forcing dataset such as a reanalysis or a global ESM. Additionally, grid nudging of temperature and wind (u and v) is applied to the top half of the model domain (above ~ 540 hPa). The lateral boundary conditions and nudging values for WRF are updated from the forcing dataset in six-hour intervals.

Modifications are made to WRF physics parameterizations, including surface layer, microphysics, cumulus, and shortwave and longwave radiation parameterizations, to work in the fully coupled model framework and to improve results in the Arctic. The selected WRF physics parameterizations are based on extensive evaluations of different combinations of parameterizations that were shown to produce the best surface state in the fully coupled RASM. The RRTMG (Iacono et al., 2008) parameterizations are used for the shortwave and longwave radiation schemes. Modifications were made to the RRTMG parameterizations to export direct and diffuse visible and near-infrared solar radiation to CPL7 and to import direct and diffuse visible and near-infrared albedo. Such partitioning of the radiation and albedo is included for use in the physics of the coupled RASM model components. The selected microphysics parameterization is the Morrison scheme (Morrison et al., 2009) with modifications to pass the droplet size to the radiation parameterizations for the calculation of radiative fluxes. The Grell 3D scheme, with shallow convection, is used for the cumulus parameterization. A modification was made to the Grell 3D scheme so that the shallow convection is only applied to the grid points over the ocean. Sub-grid cloud fraction interaction is provided by the cumulus parameterization to the radiation schemes to account for the radiative impact of the convective clouds. The planetary boundary layer parameterization is handled by the Mellor-Yamada Nakanishi and Niino Level 2.5 scheme (MYNN 2.5; Nakanishi and Niino, 2006). The integrated land model in WRF is disabled in RASM. Instead, the surface fluxes, albedo and state values are provided by the VIC, POP, and CICE component models and exchanged through the CPL7 coupler. The Revised MM5 surface layer scheme (Jiménez et al., 2012) is the selected surface layer parameterization with extensive modifications to work with the exchange of fluxes from the coupler.

The list of variables (see Cassano et al., 2017, Table 2) exchanged between WRF and the coupler in RASM is nearly identical to those passed between the atmospheric model and the coupler in CESM. The fluxes and state variables exchanged between WRF with the coupler are time-averaged over the 20-minute coupling time step. Area weighted sensible heat, latent heat, and momentum fluxes from VIC, CICE, and POP are passed to WRF for grid cells at land-ocean boundaries and/or with both sea ice and open ocean. The atmospheric surface stability is determined in CICE and CPL7 for the ice and ocean (Roberts et al., 2015) and VIC for the land (Hamman et al., 2016).

2.2 Decadal Prediction Large Ensemble

The CESM decadal prediction large ensemble (CESM-DPLE; Yeager et al., 2018) provides initial, lateral boundary, and nudging conditions for the atmospheric forcing with RASM. The DPLE provides an ensemble of initialized simulations that can be compared to the uninitialized 40-member ensemble of historical and projection (1920-2100) simulations in the CESM large ensemble (CESM-LE; Kay at al., 2015). The DPLE was created with the same CESM code base, version 1.1, component model configurations, and radiative forcing as in the CESM-LE. There are 62 1st of November start dates spanning 1954 to 2015, each with an integration of 122 months. The initial conditions for the atmosphere and land models were obtained from a single member of the CESM-LE. The ocean and sea ice initial conditions were from a coupled ocean-sea ice configuration of CESM v1.1 with historical atmospheric state and flux fields exchanged at the surface. Each DPLE start date has 40 ensemble members. The different ensemble members were generated by round-off perturbations applied to the atmospheric initial conditions. Only the initial 10 ensemble members archived the 6-hourly resolution atmospheric fields necessary for dynamical downscaling using RASM. WRF input files were created from the DPLE following that of Bruyère et al. (2015), including the WRF Preprocessing System (WPS v3.7.1) software, with modifications to some of the Bruyère et al. (2015) scripts to work with the DPLE data. The surface and sub-surface fields in the WRF input files were not necessary with RASM using a fully coupled modeling framework. Bias correction was not applied to the WRF input files from the DPLE data for reasons that will be covered in the discussion. The DPLE datasets were also regridded to the RASM atmosphere 50-km horizontal resolution domain to provide a direct comparison to the RASM simulations. These regridded datasets are hereinafter referred to as CESM-DPLE.

2.3 Reanalyses

Reanalysis datasets are used in the study to provide the initial and lateral boundary conditions, and nudging data for RASM simulations forced by reanalyses. The European Centre for Medium Range Weather Forecasts (ECMWF) Interim Re-Analysis (ERA-Interim, hereinafter referred to as ERAI; Dee et al. 2011) is the primary reanalysis used for this study. The Climate Forecast System Reanalysis (CFSR, hereinafter referred to as CFS; Saha et al., 2010b) from the National Centers for Environmental Prediction (NCEP) is used to provide a comparative reanalysis dataset and reanalysis forced RASM simulation. Lindsay et al. (2014) reviewed seven atmospheric reanalyses for the Arctic and concluded that ERAI and CFS were two of the three reanalyses that emerged as being the most consistent in comparison to observations of surface temperature, radiative fluxes, precipitation, and wind speed. The ERAI and CFS datasets were retrieved from the NCAR – Research Data Archive (NCAR-RDA; ERAI: European Centre for Medium-Range Weather Forecasts, 2009; CFS: Saha et al., 2010a). WRF input files were created from the reanalysis datasets using the WPS v3.7.1 software to convert the reanalysis source data to the WRF model domain. The ERAI and CFS datasets were also regridded to the RASM atmosphere 50-km horizontal resolution domain to provide a direct comparison to RASM simulations. The regridded datasets in the results sections are referred to as ERAI and CFS.

2.4 Experimental Setup

Two fully coupled RASM simulations forced by reanalyses, ERAI (referred to hereafter as: RASM-ERAI) and CFS (referred to as: RASM-CFS) are completed for comparisons to the DPLE-forced RASM simulations. The three-dimensional initial state of the atmosphere is from the corresponding reanalysis state of the atmosphere for 00 UTC 1 September 1979. The sea ice and ocean initial states for the fully coupled reanalysis forced RASM simulations are from a RASM ocean-sea ice simulation starting from January 1958 to August 1979 with JRA-55 forcing and runoff (Kobayashi et al., 2015). The 1 September 1979 land surface initial state is from a 31-year uncoupled VIC simulation forced with meteorological inputs (Hamman et al., 2016). The RASM POP ocean temperature and salinity, along the closed lateral boundaries, are restored to monthly values from the Polar Science Center Hydrographic Climatology version 3.0 (PHC 3.0) (Steele et al., 2001), as described in Roberts et al. (2015). The RASM-ERAI and RASM-CFS simulations were initialized on 1 September 1979 and run through 31 December 2018 and 2020, respectively. The years 1986-1995 for RASM-ERAI and RASM-CFS are analyzed in this study. Comparisons across the two reanalysis forced RASM simulations provides an understanding of the range of differences in RASM simulations when forced with approximately the same weather, as would be expected in two reanalyses.

The focus of the RASM simulations in this study is on the 10-member ensemble of RASM simulations forced by atmospheric output from the corresponding CESM-DPLE simulations with a start date of 1 December 1985. The RASM simulations were run for 121 months, through 31 December 1995 and are referred to as the RASM-DPLE ensemble. The results of this ensemble are compared to each other, a historical period to reanalyses (ERAI and CFS) spanning 1986 to 1995, RASM simulations forced by reanalyses (RASM-ERAI and RASM-CFS), and the source output from the CESM-DPLE ensemble simulations. The atmosphere in each RASM-DPLE simulation is initialized with the three-dimensional atmospheric state from the forcing data at the initial time. The land surface, ocean, and sea ice states are initialized from the RASM-ERAI simulation. The initialized values for each ensemble match the start date of the ensemble to that of the RASM-ERAI simulation. In other words, the 1 December 1985 RASM-DPLE ensemble start date uses the 00 UTC 1 December 1985 conditions from the RASM-ERAI simulation starting on 1 September 1979. Spatial two-dimensional plots of atmospheric state variables and regional plots of atmospheric state variables (not shown) were evaluated for the initial 30 days and there were no discontinuities or abrupt shifts indicated in the atmospheric analyses. This indicates that the initializations for the RASM-DPLE simulations present no need for an initial period of model spin up.

Two ensemble members from the RASM-DPLE ensemble were run a second time with a change to one of the WRF physics parameterization options to highlight the dependency of the RASM-DPLE results on the atmospheric model configuration in RASM. An additional ERAI forced RASM simulation is also run with the same WRF physics parameterization options. Past published (Cassano et al., 2017) and unpublished studies with WRF and RASM have revealed a modest change in the surface state variables and energy fluxes in the Arctic with a change in the cumulus parameterization. The alternate WRF physics configuration uses the Kain-Fritsch cumulus parameterization (Kain 2004) instead of the G3. The Kain-Fritsch scheme includes the option for including the radiative impact of clouds but it does not include the built-in shallow convection scheme as applied over ocean points with the G3 cumulus parameterization. The modified RASM simulation forced with the ERAI reanalysis is hereinafter referred to as RASM_alt-ERAI. The RASM-DPLE simulations are initialized with the land, ocean, and sea ice from 1 December 1985 conditions of the RASM_alt-ERAI simulation. These RASM-DPLE simulations are hereinafter referred to as RASM_alt-DPLE_01 and RASM_alt-DPLE_02. All RASM simulations were completed using RASM tag 2_2_01. Table 1 provides a summary of the RASM simulations used in this study.

3 Results

3.1 Intra-annual and Inter-annual Analysis of Atmospheric State

Analyses of atmospheric state variables and fluxes, on monthly and interannual time scales, reveals variability in the weather of RASM-DPLE simulations forced by the 10 CESM-DPLE ensemble members. The term weather is used in this study to denote the variation in atmospheric state as the result of the evolving patterns of the atmosphere that comprise the monthly, annual, and multiyear means. The monthly, annual, and multiyear means are not inherently weather, but it is differences in the evolution of the weather that results in differences in the respective means.

Figure 2 is a plot of RASM domain averaged atmospheric state values (height and temperature for 300, 500, 700, and 850 hPa constant pressure surfaces, sea level pressure and temperature at the surface) for the first 13 months (December 1985 to December 1986) of the 10 RASM-DPLE simulations, 2 RASM reanalysis simulations, a RASM-DPLE ensemble mean, and the forcing data. The plotted values are referred to as anomalies and are calculated as the monthly mean for the data source minus the ERAI monthly mean. The plotting of ERAI reference anomalies is used to remove the large annual cycle and allows for the variability across ensemble members to be more easily seen and it is not done in making a reference to the ERAI values as being the "truth". The left side of Figure 2 indicates the range and variability of the conditions for the 10 RASM-DPLE ensemble members for each month over the course of the initial 13 months of each simulation. The 10 ensemble members show a reasonable range of atmospheric conditions for the pan-Arctic RASM domain from the upper troposphere to the surface. RASM-DPLE_01 and RASM-DPLE_02 are plotted in red and green to highlight that these two ensemble members largely fall within the range of the overall 10 ensemble members used in this study. As is expected, these two ensemble members do, in some months, represent the upper and lower bounds of the 10 ensemble members, but overall they are not any more distinct than any of the other ensemble members.

The right side of Figure 2 compares the two selected RASM-DPLE ensemble members (01 and 02) with the corresponding CESM-DPLE ensemble members, which are providing the atmospheric forcing data. The right side also includes the monthly-means from the RASM simulations forced by reanalyses (RASM-ERAI, RASM-CFS) and the corresponding values from the reanalyses (ERAI, CFS). At 500 hPa and 300 hPa the RASM simulations (solid lines) of geopotential height and temperature closely follow the corresponding driving data (dashed lines) as is expected with nudging applied to the RASM/WRF simulations at heights approximately above 540 hPa. The differences between the DPLE ensemble members (RASM and CESM) with the reanalyses (RASM and reanalysis) shows that the ensemble members have different weather than the reanalyses, the range of which is shown in the plot of the ten ensemble members. The results at 500 and 300 hPa indicate that individual RASM simulations follow closely the weather variability in the forcing data and that there is a range of weather conditions represented across the ten ensemble members. As mentioned previously, this reference to weather is not meant in the literal sense but instead it is used to depict the variation in atmospheric patterns that when comprised together result in the differences in the plotted monthly means in Figure 2. At lower levels (700 hPa, 850 hPa, and surface) the mean RASM-DPLE geopotential height and temperature corresponds more closely to the mean values from the RASM-reanalysis simulations. The pattern of month-to-month changes in the monthly-means for the RASM-DPLE simulations tracks along the same pattern as the CESM-DPLE forcing data (following the same weather) but the actual and mean values correspond more closely to the RASM-ERAI and RASM-CFS simulations. The resultant 13-month mean for the four RASM simulations (open circles) are more similar to each other at the lower levels than their corresponding forcing data ('X' markers), unlike what is seen at upper levels (500 hPa and 300 hPa). The results for the lower part of the atmosphere and surface show that the RASM simulations develop a similar mean state, below the nudged upper portion of the model domain, but they also maintain the imprint of the weather variability (changes in monthly means due to the cumulative differences in atmospheric patterns) in the driving data.

Annual means of the atmospheric state for the two selected RASM-DPLE ensemble members, corresponding CESM-DPLE forcing data, two RASM-reanalysis simulations, and reanalyses are shown in Figure 3. The actual annual means are plotted in this figure in contrast to the ERAI referenced anomalies plotted in Figure 2. The plots on the left side of Figure 3 are the means for the entire RASM domain and the plots on the right side are the means for the Central Arctic region (see Figure 1 for region definitions). Similar to the monthly means (Figure 2), the annual mean values of geopotential height and temperature of the RASM simulations (solid lines) closely follow the respective RASM forcing data (dashed lines) at 500 hPa and 300 hPa for both the RASM domain and the Central Arctic region. There is a bias in the DPLE-based annual means (reds and greens) relative to the reanalyses-based annual means (browns and grays). For example, the DPLE-based RASM simulations and forcing data have a cold bias at 500 hPa and 300 hPa in comparison to the reanalyses-based RASM and forcing data. The pattern of the year-to-year variation of the RASM simulations matches that of the forcing data and the associated weather at 500 hPa and 300 hPa. Similarly, the 850 hPa and 700 hPa interannual patterns in geopotential height and temperature for the RASM simulations (darker colors, solid lines) correlates to the corresponding (similarly colored) forcing data (lighter colors, dashed lines) both in the RASM domain mean (left columns) and for the Central Arctic region (right columns). In contrast to the upper half of the model, where there are mean differences between the DPLE simulations/forcing data and the reanalyses simulations/forcing data, the differences in the lower half of the model separate into two clusters – one cluster for the RASM simulations, regardless of the forcing data, and another cluster for the forcing data. In some of the plots, the cluster of the forcing data is separated between the reanalyses and the CESM-DPLE forcing data, which is indicating biases in the CESM-DPLE data in comparison to the reanalyses. The differences in temperature at 700 hPa are a mixture of that from the forcing data (e.g. reanalyses are warmer than DPLE) and the RASM simulation (e.g. RASM is warmer than the forcing data) over the whole RASM domain. For the Central Arctic, there is a consistent warm bias for the RASM simulations in the lower levels (700 hPa, 850 hPa, and surface). This suggests that the RASM model physics plays a dominant role in defining a new mean climatic state in the lower levels of the atmosphere. However, the distinct interannual variability from the forcing data remains imprinted on the RASM simulations as is seen by the pattern of interannual variability of the RASM simulations following that of the forcing data. The above results demonstrate that on an annual basis the RASM-DPLE simulation reproduces the pattern of the CESM-DPLE interannual variability in geopotential height and temperature at all levels in the atmosphere. At upper levels the mean state in RASM-DPLE is very similar to that in CESM-DPLE but becomes more similar to the mean in RASM-reanalyses at the lower levels. The biases between DPLE versus reanalyses in the upper levels switches to biases between RASM simulations and forcing data in the lower levels. Similar results can be seen for the North Pacific and Lena regions (see Figure S1) in the supplementary material.

The atmospheric circulation of the RASM simulations and associated forcing data is evaluated with spaghetti plot analyses of a common single 500 hPa geopotential height (Z500, e.g. 5,400 m) plotted from each data source (Figure 4). The results show the variability and range of weather patterns for the 10 RASM-DPLE ensemble members for each month and each year. For example, each ensemble member has a 500 hPa ridge over the west coast of North America but the amplitude and position of that ridge is different for each ensemble member. The variability in the weather across the RASM-DPLE simulations remains in the annual means, although not as pronounced as in the monthly means. RASM-DPLE_01 and RASM-DPLE_02 are highlighted (red, green) and the two ensemble members are representative of the range of conditions across the ensemble, similar to what was indicated in the regional atmospheric state analyses for the ensemble (Figure 2). The results indicate that the weather at 500 hPa in the RASM simulations matches that of the forcing data with only small differences. This is as is expected for a dynamical downscaling simulation that is nudged to the forcing data for the top half of the model.

3.2 Regional Analyses Including Alternate RASM Simulations

Additional RASM simulations (RASM_alt-ERAI, RASM_alt-DPLE_01, and RASM_alt-DPLE_02) with alternate WRF physics configuration are included in the following results to highlight the role of the model's atmospheric physics. The only difference in the WRF configuration is the selection of the cumulus parameterization (see Sect. 2.4 for more details). Figure 5 is a plot of the atmospheric state for the annual cycle of monthly means across the 10 years (1986-1995) for the RASM simulations (solid lines for RASM_std and darker colors, short-dashed lines for RASM_alt) and the forcing data (lighter colors, long-dashed lines) for the RASM domain average (left side) and the Central Arctic region average (right side). (Figure S2 is the same plot but for the North Pacific and Lena regions.) The values are plotted as anomalies in reference to ERAI, as was used in Figure 2. The pattern of the annual cycle of the geopotential heights at 500 hPa and 300 hPa for the RASM simulations follows closely to that of the corresponding forcing data (similar colors) with little sensitivity to the RASM atmospheric physics configuration. This is true for the whole RASM domain and seen even more clearly for the Central Arctic region. The same characteristics in the pattern of the annual cycle and differences are seen for the temperature at 500 hPa and 300 hPa. The DPLE means indicate a cold bias, relative to ERAI, of approximately 2 °C (2 °C) at 300 hPa and 1.5 °C (0.5 °C) for the RASM domain (Central Arctic region). The pattern of the annual cycle for the RASM simulations has some deviations from that of the forcing data in temperature at 500 hPa for the Central Arctic region. This deviation is indicating the influence of the lower levels on the upper levels for the Central Arctic region. The imprint of the weather at 300 hPa and 500 hPa is present in the RASM simulations correlating to that of the forcing data, as is seen in similar patterns of variability with the RASM simulations matching that of the forcing data (similar colors). At the surface, the annual cycle of temperature displays three clusters – RASM simulations (solid lines), RASM_alt simulations (short-dashed lines) and the CESM-DPLE forcing data (long-dashed lines). The difference between the ERAI and CESM-DPLE forcing data indicating a cold bias, relative to ERAI, in surface temperature (Tsfc) for the CESM-DPLE simulations. This cold bias of Tsfc in the DPLE forcing data is completely absent in the RASM simulations, with even the annual cycle of Tsfc bias in the DPLE forcing and RASM-DPLE simulations showing different patterns. This demonstrates that the atmospheric physics of the different RASM configurations dominates the 10-year mean surface climate state. Similar comments on the patterns and biases can be made regarding the temperature at 850 hPa and 700 hPa levels, although this is not as pronounced as at the surface. At these levels the biases from the DPLE forcing is combined with the impact of the RASM model physics in determining the annual cycle in the 10-year climate.

The pattern of the 10-year annual cycle of the RASM simulations for geopotential height in the lower half of the model follows the same general pattern as the forcing data, although an offset between the RASM simulations and forcing data is evident indicating different mean values. This indicates that the differences in the weather patterns from the forcing data is still imprinted on the RASM simulations in the lower levels of the atmosphere. The Central Arctic region (righthand side of Figure 5) has slightly different levels of clustering across the RASM_std and RASM_alt simulations and the forcing data depending on the impact of the change in the RASM configuration for the Central Arctic region and time of year. The North Pacific region (Figure S2) shows the most pronounced impact on the Tsfc due to the changes in the RASM physics. Past studies (Cassano et al., 2017; Jousse et al., 2015) have found the low-level stratocumulus clouds of this region are particularly sensitive to the selection of WRF physics options.

Analyses of the fluxes at the surface emphasize the dependence of the model physics on the results for the lower atmosphere. Figure 6 is a plot of monthly means of surface temperature, precipitation, and surface fluxes for the 10-year RASM_std and RASM_alt simulations and the corresponding forcing data. The left column is the RASM domain average, and the remaining columns are that of the Central Arctic, North Pacific, and Lena region averages. The shortwave downwelling radiation (SWD; Figure 6a-d) indicates three groups of results with the individual CESM-DPLE, RASM_std, and RASM_alt simulations clustered together by simulation type (similar line style). For all but the Central Arctic, the RASM_alt simulations have the most SWD and the RASM_std simulations have the least. The longwave downwelling radiation (LWD; Figure 6e-h) also indicates the results clustered by simulation type and mostly independent of the forcing data, with the order of the biases in the LWD differing by region. The sum of sensible heat and latent heat (SH + LH; Figure 6i-l) does not show as clearly discernible characteristics as SWD and LWD but there are similar features. For example, the three simulations with the smallest SH + LH values for the North Pacific are RASM_std simulations and the three largest SH + LH values for the Lena region are RASM_alt simulations. Similar comments are true with precipitation (Figure 6m-p) with RASM_std (RASM_alt) having the three largest means of precipitation for the North Pacific (Lena) region and the CESM-DPLE simulations having the three smallest means of precipitation for the Central Arctic and Lena regions. The plots of surface temperature (Figure 6q-t) highlight the cold bias of the CESM-DPLE simulations in comparison to ERAI and a warm bias for nearly all RASM simulations in comparison to ERAI. The results in analyzing the surface fluxes, precipitation and temperature indicate that the model physics plays the largest role in the climate of the surface energy fluxes and atmospheric state in the lower atmosphere. A change in the WRF physics parameterizations (e.g. planetary boundary layer, microphysics, and cumulus parameterizations) will produce a different mean climatic state no matter the forcing data.

3.3 Spatial Analyses of Atmospheric State and Surface Fluxes

Analyses of spatial patterns of Z500, LWD, and Tsfc, with annual and seasonal (December-January-February, DJF; June-July-August, JJA) means for 1986, provide additional understanding of the similarities and differences in the RASM simulations and forcing data. The differences of Z500 (Figure 7), between RASM simulations and forcing data, provides a greater understanding of the relative dependencies with the dynamical downscaling using RASM. There are minimal differences in Z500 between the RASM simulation and forcing data (ERAI, Figure 7a; DPLE_01, Figure 7c). These results are similar to what was indicated previously with the regional plots of atmospheric state (Figs. 3 and 5) and the Z500 (Figure 4). This is also true for the RASM_alt simulation with changes in WRF physics (RASM_alt-ERAI – RASM-ERAI, Figure 7b). This indicates that the atmospheric circulation for the top half of the RASM model is constrained by the nudging to the forcing data, as is expected. Meanwhile, the differences in the weather between the DPLE_01 and ERAI forcing data (CESM-DPLE_01 – ERAI, Figure 7e) are reflected with similar patterns of differences between RASM simulations dependent on forcing data (RASM-DPLE_01 – RASM-ERAI, Figure 7d) and in comparing the RASM-DPLE_01 simulation to ERAI (RASM-DPLE_01 – ERAI, Figure 7f). The differences in Z500 represent the changes in the atmospheric circulation for the top half of the RASM simulations between DPLE_01 and ERAI. The results for the temperature at 500 hPa (Figure S3) show similar results with minimal differences indicated between the RASM simulation and its forcing data and larger differences when comparing results between DPLE_01 and ERAI, in either the RASM simulation and/or the forcing data.

The spatial differences in LWD across the RASM simulations and forcing data (Figure 8) highlight the predominant dependence of RASM and the model physics on the results for LWD. The differences in LWD in RASM-ERAI and ERAI (Figure 8a) indicate that RASM has more LWD compared to ERAI over almost the entire RASM domain. This is an inherent RASM bias in relation to ERAI. Similar differences in LWD are found in the comparison between the RASM-DPLE_01 and ERAI (Figure 8f) highlighting the dominance of the inherent RASM biases over the differences in weather for 1986 between DPLE_01 and ERAI. A comparison of RASM with the alternate WRF physics and the RASM standard configuration (Figure 8b) indicates that the change in WRF physics results in a decrease in LWD across the entire ocean regions of the RASM domain for the annual mean and the winter mean. The results also indicate a decrease in LWD over land downwind of the ocean regions. There is less difference for the summer months of 1986 over the RASM region, except for the lower-latitude ocean. Meanwhile the results for LWD radiation between RASM simulations with different forcing data (Figure 8d) indicate relatively small differences, in comparison to that of differences in the modeling systems (Figure 9a-9c), across the RASM domain for the annual and seasonal means, except for the Central Arctic in the winter. These results highlight that the model physics plays a larger role on the annual and seasonal means than the differences in weather for 1986 but the difference in weather still has a small imprint. A comparison of LWD in CESM-DPLE_01 and ERAI (Figure 8e) indicates that CESM has seasonally varying differences in LWD in relation to ERAI. These differences are similar for CESM-DPLE_01 (Figure 8d) and CESM-DPLE_02 (not shown) indicating that these are inherent differences in CESM relative to ERAI, are most dependent on the differences in model physics (CESM vs ERAI) and less so due to the differences in the weather. A similar analysis of SWD (Figure S5) shows results indicating that the SWD is largely a function of the model physics (CESM / RASM vs ERAI and RASM_alt vs RASM) with some regional sensitivity to the driving data (ERAI versus DPLE_01). These results for LWD (Figure 8) and SWD (Figure S4) are opposite of that for the Z500 (Figure 7) indicating the larger role that the model biases, and model physics, have on the downwelling radiation at the surface, in comparison to changes in the weather of the simulations (forcing data).

Comparisons of spatial differences of Tsfc across the different RASM simulations and forcing data for 1986 (Figure 9) show varying dependencies related to changes in the forcing data (weather), model and changes in modeling system/physics. The differences in Tsfc between RASM-ERAI and ERAI (Figure 9a) indicate that RASM has a warm bias over most land areas and a slight cold bias over the sub-polar oceans (year-round) and a cold bias over the central Arctic (DJF). These differences reflect RASM's preferred climate state, or inherent model biases in comparison to ERAI. At least a part of the positive Tsfc biases are likely associated with the positive differences in LWD at the surface (Figure 9a). The comparison of CESM-DPLE_01 and ERAI (Figure 9e) shows that CESM-DPLE_01 has a cold bias relative to ERAI in most areas (annually and DJF) but some regional warm biases in the summer. The differences in this comparison reflect both the inherent biases in CESM Tsfc relative to ERAI and the differences in seasonal and annual weather for this ensemble member compared to the weather in ERAI for 1986. These cold biases for CESM in relation to ERAI were previously indicated in the regional plots for the RASM domain and the Central Arctic (Figure 3r,t). The Tsfc in RASM-DPLE_01 relative to RASM-ERAI (Figure 9d) reflects the unique weather of this ensemble member in relation to ERAI for the specific seasons and year for 1986. A comparison of differences in Tsfc between RASM simulations with the modified WRF physics and that of the standard RASM configuration (Figure 9b) shows a slight warm difference across the North Pacific, western Siberia, eastern Canada, and the north Atlantic for the annual mean. RASM_alt-ERAI has a slight cool difference relative to RASM-ERAI over the land areas for the DJF mean. Meanwhile for JJA there are moderate warm differences across the entire RASM domain, except the Central Arctic. The Tsfc differences between RASM_alt and RASM_std (Figure 9b) are slightly smaller in magnitude than the differences between RASM-ERAI and ERAI (Figure 9a) indicating that even a single change in the model physics can significantly alter the Tsfc. In summary, the results for Tsfc across the RASM simulations and forcing data for 1986 (Figure 9) indicate a reverse of that of Z500 (Figure 7) with changes in model system (panels: a, c in Figs. 7 and 9) and changes in model configuration (panels: b) presenting larger differences than the changes in weather (DPLE ensemble members or ERAI, panels: d). Spatial plots of Tsfc differences for the DPLE_02 ensemble member (CESM-DPLE_02, RASM-DPLE_02) in comparison to forcing data, the DPLE_01 ensemble member, and modifications to the WRF physics are provided in Figure S5 to further highlight these conclusions.

3.4 Evaluation of Sea Ice and Ocean Transport in the RASM-DPLE Ensemble

The analyses presented above demonstrate that the dynamical downscaling of the CESM-DPLE ensemble members by RASM results in the top half of the model following that of the forcing data as a result of using nudging in RASM. In contrast, the near surface state and radiative fluxes are clustered more closely among modeling systems (CESM, RASM, and reanalyses), and model configuration (RASM_std vs RASM_alt) than due to the differences in the weather (forcing data: reanalyses and DPLE ensemble members). Despite the strong control the modeling system and model configuration have on near surface state and radiative fluxes there is still a signal from differences in weather across the different forcing data. As a result the fully-coupled RASM simulations display differences in sea ice and oceanic transport that varies with forcing data.

Figure 10 is a spatial plot showing sea ice extent for the RASM simulations and NSIDC sea ice observations for March 1995 (Figure 10a,c) and September 1995 (Figure 10b,d), representing the results 10 years into the RASM-DPLE simulations. The top two panels (Figure 10a,b) show all 10 RASM-DPLE ensemble members and the ensemble mean. The Chukchi, East Siberian, and Laptev seas in particular shows large variations in the sea ice extent for September 1995 (Figure 10b) depending on the evolution of weather in a given DPLE ensemble member. The impact of the changes in WRF physics in RASM (RASM_alt) simulations going to a different surface climate state are indicated in the lower panels (Figure 10c,d) with the dashed lines indicating the modified WRF physics. For March 1995 (Figure 10c) the RASM_alt simulations for the same ensemble member have a slightly larger sea ice extent than the corresponding RASM_std simulations for the same ensemble member (similar color). The sea ice extent for the RASM_alt simulations is less than that of the RASM_std simulations for September 1995 (Figure 10d). This is reflective of the warmer Tsfc conditions during JJA in the RASM_alt simulations than the RASM simulations as previously indicated in Figure 6q-t and Figure 9b over the western Arctic.

Figure 11 is a time series plot of sea ice volume from the RASM simulations and PIOMAS (Schweiger et al. 2011; Zhang and Rothrock 2003) reference values from 1986 to 1995. The top panel (Figure 11a) shows the range of sea ice volume across the 10 RASM-DPLE ensemble members from 1986 to 1995, once again showing that despite RASM model producing a similar near-surface climate state for the 10 years across the ensemble members the evolution of the weather results in different sea ice results across the RASM-DPLE ensemble members. A review of the differences in RASM simulations with and without modified WRF physics (Figure 11b) shows that in general the modified WRF physics output is resulting in less sea ice in the fully coupled RASM simulations. Hence, the modification in the WRF physics accounts for a change in the fully coupled sea ice conditions. It can also be seen that the decadal trend between the RASM_std and RASM_alt simulations for each ensemble member are similar.

The impacts of the different DPLE ensemble members on the RASM fully coupled climate system extend to that of oceanic volume transport. Figure 12 shows the net volume transport across two main gateways between the North Atlantic and the Arctic Ocean: the Barents Sea Opening (Figure 12a,c) and Fram Strait (Figure 12b,d). The top two panels (Figure 12a,b) are more chaotic than that of sea ice volume (Figure 11) but shows the same story with each ensemble member representing part of the range of results for volume transport between the Barents Sea Opening and Fram Strait. At times a given ensemble member will have the largest amount of volume transport for a given month and at times that same ensemble member will have the least. The comparison of the RASM_std and RASM_alt simulations (Figure 12c,d) show comparable variability with the RASM_std simulations (solid lines) representing higher volume transport across the Barents Sea Opening compared to that from the RASM_alt simulations (dashed lines).

4 Discussion and Conclusions

This study has evaluated the results of the dynamical downscaling of ESM and reanalysis data by the fully coupled RASM. This version of RASM has atmosphere, land, ocean, and sea ice component models that exchange fluxes and state values through a coupler. For this dynamical downscaling study, the land, ocean, and sea ice were initialized by a previous RASM simulation forced by the ERAI reanalysis. After the initialization, the land, ocean, and sea ice models evolve freely based on the interactions with the atmosphere and the respective model evolution. This contrasts with the more frequently used dynamical downscaling with an atmosphere-only model that has prescribed lower boundary conditions from either the forcing ESM or a secondary dataset, such as satellite observations of sea surface temperature. The ability for RASM to evolve at the surface more freely, without prescribed lower-boundary conditions, highlights one of the unique aspects of this study.

Here, we have created an ensemble of RASM simulations using 10 members of the CESM-DPLE, two reanalyses, and two versions of RASM that differ in their model physics. This ensemble of RASM simulations allows us to evaluate the relative role of differences in weather, differences due to biases in the driving data, and differences due to changes in the modeling system. The first 10 ensemble members of the CESM-DPLE project, with a start date of 1 November 1985, are used to provide the ESM forcing data for the dynamical downscaling in RASM. An advantage to using 10 ensemble members from the CESM-DPLE is that it allows for an evaluation of differences due solely to changes in the weather across the 10 ensemble members. The term weather in this context is used to denote the temporal variation in atmospheric state as the result of the evolving atmospheric patterns that produce the monthly, annual, and multiyear means. Two RASM simulations were completed using the ERAI and CFS reanalyses running from September 1979 through 2018 (2020 for CFS). Comparison of the reanalysis forced RASM simulations with the DPLE forced simulations allows for an assessment of the impact of biases in the driving data (CESM-DPLE) on the downscaled climate state. An alternate RASM configuration (RASM_alt) was configured with a change in the selected cumulus parameterization in the WRF model. The RASM_alt configuration is used to highlight the dependency of the results on the configuration of the atmospheric model in RASM.

The analyses presented here focus on time series of monthly, annual, and multiyear means of the atmospheric climatic state at all levels of the atmosphere across the 10 RASM-DPLE ensemble members, two reanalyses, and RASM_alt simulations. Additionally, Z500 spaghetti plots, and spatial plots of Z500, LWD, and Tsfc are used to assess the range of results across all RASM simulations and forcing data. Two ensemble members (01 and 02) were selected for a more careful examination with a comparison to the reanalyses and the corresponding CESM-DPLE forcing data. The RASM simulations of the two ensemble members and the two reanalyses indicate that for the 300 hPa and 500 hPa geopotential height and temperature fields the mean climatic state matches that of the corresponding forcing data (either reanalysis or CESM-DPLE). This is the expected result for dynamical downscaling simulations where nudging to the forcing data is applied to the top half of the model. The position and amplitude of ridges and troughs of geopotential height at 500 hPa for any given month or year also indicate a strong correlation between the RASM simulations and the forcing data (Figure 4). The results indicate that there are biases of lower temperatures and lower geopotential heights in the DPLE results, for both CESM and RASM, in comparison to the reanalyses (ERAI and CFS).

Meanwhile, the results of the mean climatic state, as indicated in the annual and multi-year means, for the lower half of the atmosphere tend to form three clusters: i) RASM simulations with either CESM or reanalysis forcing data, ii) CESM-DPLE, and iii) reanalyses. RASM and CESM both have biases relative to the reanalyses, but RASM-DPLE simulation biases are unique from the biases in the CESM-DPLE forcing data used for these simulations and are similar to the RASM-ERAI biases. For example, monthly means of Tsfc for the 10-year simulations across the RASM domain show the RASM simulations (DPLE and reanalysis) with a warm bias in relation to ERAI and the CESM-DPLE forcing data as a cold bias in relation to ERAI (Figure 6r). The biases that are present in the CESM-DPLE forcing data are no longer present in the RASM-DPLE simulations.

The mean climatic state of the lower part of the RASM atmosphere is largely independent of the nudging to the forcing data and is instead dependent on RASM's inherent biases, atmospheric physics parameterizations, and presumably resolution, in driving the near surface state in the model. The RASM_alt simulations result in a different mean state of the lower atmosphere and surface as indicated by Tsfc and the surface fluxes (Figure 6) because of the change of a single physics parameterization (the cumulus parameterization). The changes in the forcing data (across DPLE ensemble members or in comparison to the reanalyses) are not large enough to change the clouds and fluxes that form the mean RASM climatic state for the lower atmosphere and surface.

Bias correction to ESM data is a common prerequisite in using ESM output for forcing of RCMs. In this study it was found that the bias correction of the ESM data was not necessary in the fully coupled modeling framework. There is a level of independence between the upper half of the model domain, where nudging is applied to the forcing data, and what happens at the surface in that the biases in the DPLE temperature have no, or insignificant, impact on the results for the lowest part of the atmosphere. Instead, it is the physics parameterizations of the atmospheric model that play the dominant role in establishing the mean climatic state of the lower atmosphere and near surface conditions. The results indicate that it is possible to do downscaling with a biased ESM and obtain reasonable and improved results at the surface. The key difference as to why this is the case for this study, in contrast to previous studies with an atmosphere-only RCM framework, is that the surface conditions are not prescribed by the ESM forcing data but evolve freely through coupling between the atmosphere and the other component models.

The results indicate that despite the mean surface climatic state, as indicated by annual and multi-year means, being similar across the ensemble of 10-year RASM-DPLE simulations there are differences in how the model reaches that mean climatic state. Those differences are in the evolution of the weather, or the sequence and intensity of the atmospheric circulation, over the 10 years that produce the mean climatic state. These differences in weather are indicated in the month-to-month patterns of the monthly means (Figure 2), the year-to-year patterns in annual means (Figure 3), and the differences in the position and amplitude of the ridges and troughs in the 500 hPa geopotential spaghetti plots (Figure 4). The RASM-DPLE simulations produce weather that is unique for each ensemble member, and that is consistent with the CESM-DPLE driving data as indicated by similar month-to-month and year-to-year patterns in the analyses (Figs. 2, 3, and 5). The differences in the evolution of the weather across the 10 ensemble members results in variances in the sea ice state (Figs. 10 and 11), and the oceanic transport into and out of the Arctic (Figure 12). Despite having a similar mean climatic state across the ensemble members the sea ice and oceanic states are different across the RASM ensemble members. This is similar to how there are differences in sea ice and oceanic states from year-to-year in recent history despite the minimal differences in the year-to-year mean climatic state.

The benefits of a fully coupled RESM lie in the ability of the model to respond to the larger scale weather, accomplished through the nudging to the ESM or reanalysis forcing data, meanwhile the higher spatial and temporal resolution in combination with the more region-specific and flexible atmospheric physics in the RESM allows the lower portion of the atmosphere and the coupled model components to freely evolve, largely independent of the forcing data. Changes or improvements to a RESM atmospheric physics impact the mean climatic state of the atmospheric and coupled components of the RESM. In the case of RASM, the Arctic-optimized configuration of the ocean model, and the higher spatial and temporal resolutions of the ocean and sea ice models, allow for a more realistic representation of the physical processes and mechanisms for the Arctic climate system.

Acknowledgments

This research was supported by the Regional and Global Model Analysis (RGMA) component of the Earth and Environmental System Modeling (EESM) program of the U.S. Department of Energy's Office of Science, as contribution to the HiLAT-RASM project. Computing resources for the RASM simulations were provided by the U.S. DOD High Performance Computer Modernization Program (HPCMP). The CESM-DPLE was generated using computational resources provided by the National Energy Research Scientific Computing Center (NERSC), which is supported by the Office of Science of the U.S. Department of Energy. The CESM-DPLE data was retrieved through the NERSC data portal.

Open Research

The reanalysis data used in this study was retrieved from the Research Data Archive at the National Center for Atmospheric Research (NCAR), Computational and Information Systems Laboratory (https://rda.ucar.edu/). The CESM-DPLE data used in this study was retrieved through the NCAR CESM community project website (https://www.cesm.ucar.edu/community-projects/dple). All RASM simulations are archived in the HPCMP archive system and will be available upon publication according to the U.S. DoD data policy.

References

Bowden, J. H., Otte, T. L., Nolte, C. G., & Otte, M. J. (2012). Examining Interior Grid Nudging Techniques Using Two-Way Nesting in the WRF Model for Regional Climate Modeling. *Journal of Climate*, *25*(8), 2805–2823. https://doi.org/10.1175/jcli-d-11-00167.1

Bruyère, C. L., Done, J. M., Holland, G. J., & Fredrick, S. (2013). Bias corrections of global models for regional climate simulations of high-impact weather. *Climate Dynamics*, *43*(7–8), 1847–1856. https://doi.org/10.1007/s00382-013-2011-6

Bruyère, C. L., Monaghan, A. J., Steinhoff, D. F., & Yates, D. (2015). *Bias-Corrected CMIP5 CESM Data in WRF/MPAS Intermediate File Format* (No. NCAR/TN 515+STR) (p. 27). Boulder, CO: National Center for Atmospheric Research.

Bullock, O. R. J., Alapaty, K., Herwehe, J. A., Mallard, M. S., Otte, T. L., Gilliam, R. C., & Nolte, C. G. (2014). An Observation-Based Investigation of Nudging in WRF for Downscaling

Surface Climate Information to 12-km Grid Spacing. *Journal of Applied Meteorology and Climatology*, *53*(1), 20–33. https://doi.org/10.1175/jamc-d-13-030.1

Cassano, J. J., Higgins, M. E., & Seefeldt, M. W. (2011). Performance of the Weather Research and Forecasting Model for Month-Long Pan-Arctic Simulations. *Monthly Weather Review*, *139*(11), 3469–3488. https://doi.org/10.1175/mwr-d-10-05065.1

Cassano, J. J., DuVivier, A., Roberts, A., Hughes, M., Seefeldt, M., Brunke, M., et al. (2017). Development of the Regional Arctic System Model (RASM): Near-Surface Atmospheric Climate Sensitivity. *Journal of Climate*, JCLI-D-15-0775.1. https://doi.org/10.1175/jcli-d-15-0775.1

Craig, A. P., Vertenstein, M., & Jacob, R. (2012). A new flexible coupler for earth system modeling developed for CCSM4 and CESM1. *The International Journal of High Performance Computing Applications*, *26*(1), 31–42. https://doi.org/10.1177/1094342011428141

Dee, D. P., Uppala, S. M., Simmons, A. J., Berrisford, P., Poli, P., Kobayashi, S., et al. (2011). The ERA-Interim reanalysis: configuration and performance of the data assimilation system. *Quarterly Journal of the Royal Meteorological Society*, *137*(656), 553–597. https://doi.org/10.1002/qj.828

European Centre for Medium-Range Weather Forecasts: ERA-Interim Project (2009). Research Data Archive at the National Center for Atmospheric Research, Computational and Information Systems Laboratory. Last accessed 28 April 2020. https://doi.org/10.5065/D6CR5RD9

Giorgi, F. (2019). Thirty Years of Regional Climate Modeling: Where Are We and Where Are We Going next? *Journal of Geophysical Research: Atmospheres*, *124*, 5696–5723. https://doi.org/10.1029/2018jd030094

Giorgi, F., & Gao, X.-J. (2018). Regional earth system modeling: review and future directions. *Atmospheric and Oceanic Science Letters*, *11*(2), 1–9. https://doi.org/10.1080/16742834.2018.1452520

Glisan, J. M., Gutowski, W. J. J., Cassano, J. J., & Higgins, M. E. (2013). Effects of Spectral Nudging in WRF on Arctic Temperature and Precipitation Simulations. *Journal of Climate*, *26*(12), 3985–3999. https://doi.org/10.1175/jcli-d-12-00318.1

Gutowski, W. J., Ullrich, P. A., Hall, A., Leung, L. R., O'Brien, T. A., Patricola, C. M., et al. (2020). The ongoing need for high-resolution regional climate models: Process understanding and stakeholder information. *Bulletin of the American Meteorological Society*, *101*(5), E664–E683. https://doi.org/10.1175/bams-d-19-0113.1

Hamman, J., Nijssen, B., Brunke, M., Cassano, J., Craig, A., DuVivier, A., et al. (2016). Land Surface Climate in the Regional Arctic System Model. *Journal of Climate*, *29*(18), 6543–6562. https://doi.org/10.1175/jcli-d-15-0415.1

Hamman, J., Nijssen, B., Roberts, A., Craig, A., Maslowski, W., & Osinski, R. (2017). The coastal streamflow flux in the Regional Arctic System Model. *Journal of Geophysical Research: Oceans*, *122*(3), 1683–1701. https://doi.org/10.1002/2016jc012323

Hoffmann, P., Katzfey, J. J., McGregor, J. L., & Thatcher, M. (2016). Bias and variance correction of sea surface temperatures used for dynamical downscaling. *Journal of Geophysical Research: Atmospheres*, *121*(21), 12,877-12,890. https://doi.org/10.1002/2016jd025383

Hunke, E., Allard, R., Bailey, D. A., Blain, P., Craig, A., Damsgaard, A., et al. (2018). CICE-Consortium/CICE: CICE version 6.0.0 (CICE6.0.0). *Zenodo*. https://doi.org/10.5281/zenodo.1900639

Hurrell, J. W., Holland, M. M., Gent, P. R., Ghan, S., Kay, J. E., Kushner, P. J., et al. (2013). The Community Earth System Model: A Framework for Collaborative Research. *Bulletin of the American Meteorological Society*, *94*(9), 1339–1360. https://doi.org/10.1175/bams-d-12-00121.1

Iacono, M. J., Delamere, J. S., Mlawer, E. J., Shephard, M. W., Clough, S. A., & Collins, W. D. (2008). Radiative forcing by long-lived greenhouse gases: Calculations with the AER radiative transfer models. *Journal of Geophysical Research: Atmospheres (1984–2012)*, *113*(D13). https://doi.org/10.1029/2008jd009944

Jiménez, P. A., Dudhia, J., González-Rouco, J. F., Navarro, J., Montávez, J. P., & García-Bustamante, E. (2012). A Revised Scheme for the WRF Surface Layer Formulation. *Monthly Weather Review*, *140*(3), 898–918. https://doi.org/10.1175/mwr-d-11-00056.1

Jousse, A., Hall, A., Sun, F., & Teixeira, J. (2015). Causes of WRF surface energy fluxes biases in a stratocumulus region. *Climate Dynamics*, *46*(1–2), 571–584. https://doi.org/10.1007/s00382-015-2599-9

Kain, J. S. (2004). The Kain–Fritsch Convective Parameterization: An Update. *Journal of Applied Meteorology*, *43*(1), 170–181. https://doi.org/10.1175/1520-0450(2004)043<0170:tkcpau>2.0.co;2

Kay, J. E., Deser, C., Phillips, A., Mai, A., Hannay, C., Strand, G., et al. (2015). The Community Earth System Model (CESM) Large Ensemble Project: A Community Resource for Studying Climate Change in the Presence of Internal Climate Variability. *Bulletin of the American Meteorological Society*, *96*(8), 1333–1349. https://doi.org/10.1175/bams-d-13-00255.1

Kinney, J. C., Maslowski, W., Osinski, R., Jin, M., Frants, M., Jeffery, N., & Lee, Y. J. (2020). Hidden Production: On the Importance of Pelagic Phytoplankton Blooms Beneath Arctic Sea Ice. *Journal of Geophysical Research: Oceans*, *125*(9). https://doi.org/10.1029/2020jc016211

Kobayashi, S., Ota, Y., Harada, Y., Ebita, A., Moriya, M., Onoda, H., et al. (2015). The JRA-55 Reanalysis: General Specifications and Basic Characteristics. *Journal of the Meteorological Society of Japan. Ser. II*, *93*(1), 5–48. https://doi.org/10.2151/jmsj.2015-001

Liang, X., Lettenmaier, D. P., Wood, E. F., & Burges, S. J. (1994). A simple hydrologically based model of land surface water and energy fluxes for general circulation models. *Journal of Geophysical Research: Atmospheres*, *99*(D7), 14415–14428. https://doi.org/10.1029/94jd00483

Liang, X., Wood, E. F., & Lettenmaier, D. P. (1996). Surface soil moisture parameterization of the VIC-2L model: Evaluation and modification. *Global and Planetary Change*, *13*(1–4), 195–206. https://doi.org/10.1016/0921-8181(95)00046-1

Lindsay, R., Wensnahan, M., Schweiger, A., & Zhang, J. (2014). Evaluation of Seven Different Atmospheric Reanalysis Products in the Arctic*. *Journal of Climate*, *27*(7), 2588–2606. https://doi.org/10.1175/jcli-d-13-00014.1

Liu, P., Tsimpidi, A. P., Hu, Y., Stone, B., Russell, A. G., & Nenes, A. (2012). Differences between downscaling with spectral and grid nudging using WRF. *Atmospheric Chemistry and Physics*, *12*(8), 3601–3610. https://doi.org/10.5194/acp-12-3601-2012

Maslowski, W., Kinney, J. C., Higgins, M., & Roberts, A. (2012). The Future of Arctic Sea Ice. *Annual Review of Earth and Planetary Sciences*, *40*(1), 625–654. https://doi.org/10.1146/annurev-earth-042711-105345

Morrison, H., Thompson, G., & Tatarskii, V. (2009). Impact of Cloud Microphysics on the Development of Trailing Stratiform Precipitation in a Simulated Squall Line: Comparison of One- and Two-Moment Schemes. *Monthly Weather Review*, *137*(3), 991–1007. https://doi.org/10.1175/2008mwr2556.1

Nakanishi, M., & Niino, H. (2006). An Improved Mellor–Yamada Level-3 Model: Its Numerical Stability and Application to a Regional Prediction of Advection Fog. *Boundary-Layer Meteorology*, *119*(2), 397–407. https://doi.org/10.1007/s10546-005-9030-8

Powers, J. G., Klemp, J. B., Skamarock, W. C., Davis, C. A., Dudhia, J., Gill, D. O., et al. (2017). The Weather Research and Forecasting Model: Overview, System Efforts, and Future Directions. *Bulletin of the American Meteorological Society*, *98*(8), 1717–1737. https://doi.org/10.1175/bams-d-15-00308.1

Roberts, A., Craig, A., Maslowski, W., Osinski, R., DuVivier, A., Hughes, M., et al. (2015). Simulating transient ice–ocean Ekman transport in the Regional Arctic System Model and Community Earth System Model. *Annals of Glaciology*, *56*(69), 211–228. https://doi.org/10.3189/2015aog69a760

Saha, S., Moorthi, S., Pan, H., Wu, X., Wang, J., Nadiga, S., et al. (2010a). NCEP Climate Forecast System Reanalysis (CFSR) 6-hourly Products, January 1979 to December 2010, Research Data Archive at the National Center for Atmospheric Research, Computational and Information Systems Laboratory. Last accessed 18 May 2020. https://doi.org/10.5065/D69K487J

Saha, S., Moorthi, S., Pan, H.-L., Wu, X., Wang, J., Nadiga, S., et al. (2010b). The NCEP Climate Forecast System Reanalysis. *Bulletin of the American Meteorological Society*, *91*(8), 1015–1058. https://doi.org/10.1175/2010bams3001.1

Schweiger, A., Lindsay, R., Zhang, J., Steele, M., Stern, H., & Kwok, R. (2011). Uncertainty in modeled Arctic sea ice volume. *Journal of Geophysical Research*, *116*(C8). https://doi.org/10.1029/2011jc007084

Sitz, L. E., Sante, F. D., Farneti, R., Fuentes-Franco, R., Coppola, E., Mariotti, L., et al. (2017). Description and evaluation of the Earth System Regional Climate Model (Reg CM-ES). *Journal of Advances in Modeling Earth Systems*, *9*(4), 1863–1886. https://doi.org/10.1002/2017ms000933

Skamarock, W. C., Klemp, J. B., Dudhia, J., Gill, D. O., Barker, D., Duda, M. G., et al. (2008). *A Description of the Advanced Research WRF Version 3* (NCAR Technical Note No. NCAR/TN–475+STR) (p. 113). University Corporation for Atmospheric Research. Retrieved from doi:10.5065/D68S4MVH

Smith, R., Jones, P., Bryan, F., Danabasoglu, G., Dennis, J., Dukowicz, J., et al. (2010). *The Parallel Ocean Program (POP) Reference Manual Ocean Component of the Community Climate System Model (CCSM) and Community Earth System Model (CESM)* (No. LAUR-10-01853) (p. 140). Los Alamos, NM: Los Alamos National Laboratory. Retrieved from https://www.cesm.ucar.edu/models/cesm2/ocean/doc/sci/POPRefManual.pdf

Steele, M., Morley, R., & Ermold, W. (2001). PHC: A Global Ocean Hydrography with a High-Quality Arctic Ocean. *Journal of Climate*, *14*(9), 2079–2087. https://doi.org/10.1175/1520-0442(2001)014<2079:pagohw>2.0.co;2

White, R. H., & Toumi, R. (2013). The limitations of bias correcting regional climate model inputs. *Geophysical Research Letters*, *40*(12), 2907–2912. https://doi.org/10.1002/grl.50612

Xu, Z., & Yang, Z.-L. (2015). A new dynamical downscaling approach with GCM bias corrections and spectral nudging. *Journal of Geophysical Research: Atmospheres*, *120*(8), 3063–3084. https://doi.org/10.1002/2014jd022958

Xu, Z., Han, Y., Tam, C.-Y., Yang, Z.-L., & Fu, C. (2021). Bias-corrected CMIP6 global dataset for dynamical downscaling of the historical and future climate (1979–2100). *Scientific Data*, *8*(1), 293. https://doi.org/10.1038/s41597-021-01079-3

Yeager, S. G., Danabasoglu, G., Rosenbloom, N., Strand, W., Bates, S., Meehl, G., et al. (2018). Predicting near-term changes in the Earth System: A large ensemble of initialized decadal prediction simulations using the Community Earth System Model. *Bulletin of the American Meteorological Society*, *99*(9), 1867–1886. https://doi.org/10.1175/bams-d-17-0098.1

Yu, X., Rinke, A., Dorn, W., Spreen, G., Lüpkes, C., Sumata, H., & Gryanik, V. M. (2020). Evaluation of Arctic sea ice drift and its dependency on near-surface wind and sea ice conditions in the coupled regional climate model HIRHAM–NAOSIM. *The Cryosphere*, *14*(5), 1727–1746. https://doi.org/10.5194/tc-14-1727-2020

Zhang, J., & Rothrock, D. A. (2003). Modeling Global Sea Ice with a Thickness and Enthalpy Distribution Model in Generalized Curvilinear Coordinates. *Monthly Weather Review*, *131*(5), 845–861. https://doi.org/10.1175/1520-0493(2003)131<0845:mgsiwa>2.0.co;2

Tables

Table 1. List of RASM simulations with the simulation name, forcing data, initial date, end date, and specification of the WRF physics in RASM.

RASM Simulations

Title	Forcing data	Initial date	End date	WRF physics
RASM-ERAI	ERAI	1 Sept. 1979	31 Dec. 2018	RASM default
RASM-CFS	CFS	1 Sept. 1979	31 Dec. 2020	RASM default
RASM-DPLE_01, _02, _03, …, _10	CESM-DPLE_01, _02, _03, …, _10	1 Dec. 1985	31 Dec. 1995	RASM default
RASM_alt-ERAI	ERAI	1 Sept. 1979	31 Dec. 1995	Cu = Kain-Fritsch
RASM_alt-DPLE_01, _02	CESM-DPLE_01, _02	1 Dec. 1985	31 Dec. 1995	Cu = Kain-Fritsch

Figures with captions.

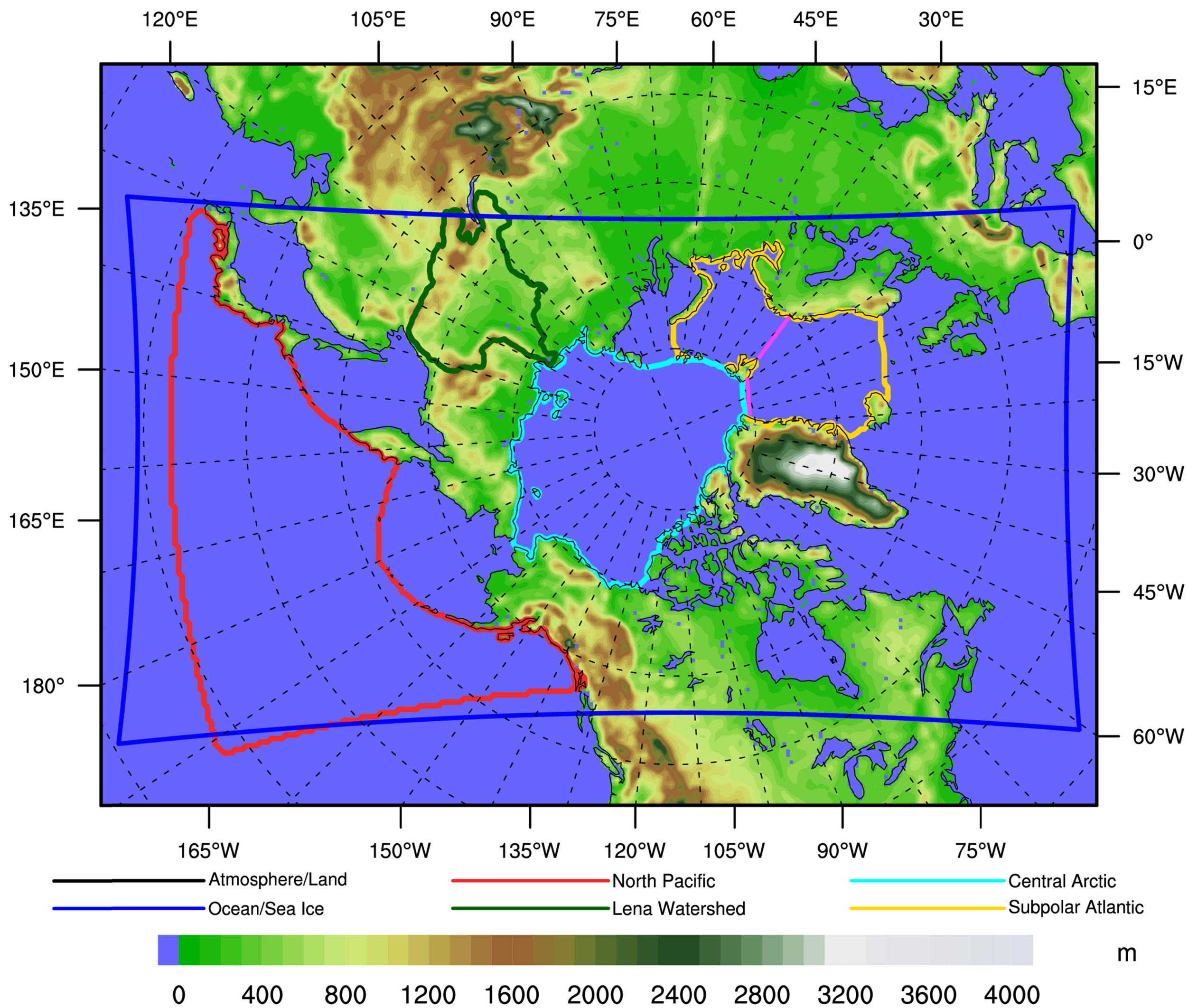

Figure 1. RASM model domains, topography, and analysis regions. The 50-km atmosphere / land domain covers the entire map region. The 9-km ocean / sea ice domain is indicated by the blue line. The North Pacific, Lena Watershed, Central Arctic, and Subpolar Atlantic analysis regions are outlined in red, dark green, cyan, and yellow. The color bar indicates the topography contours. The Fram Strait and Barents Sea Opening gateways for oceanic transport are indicated in magenta.

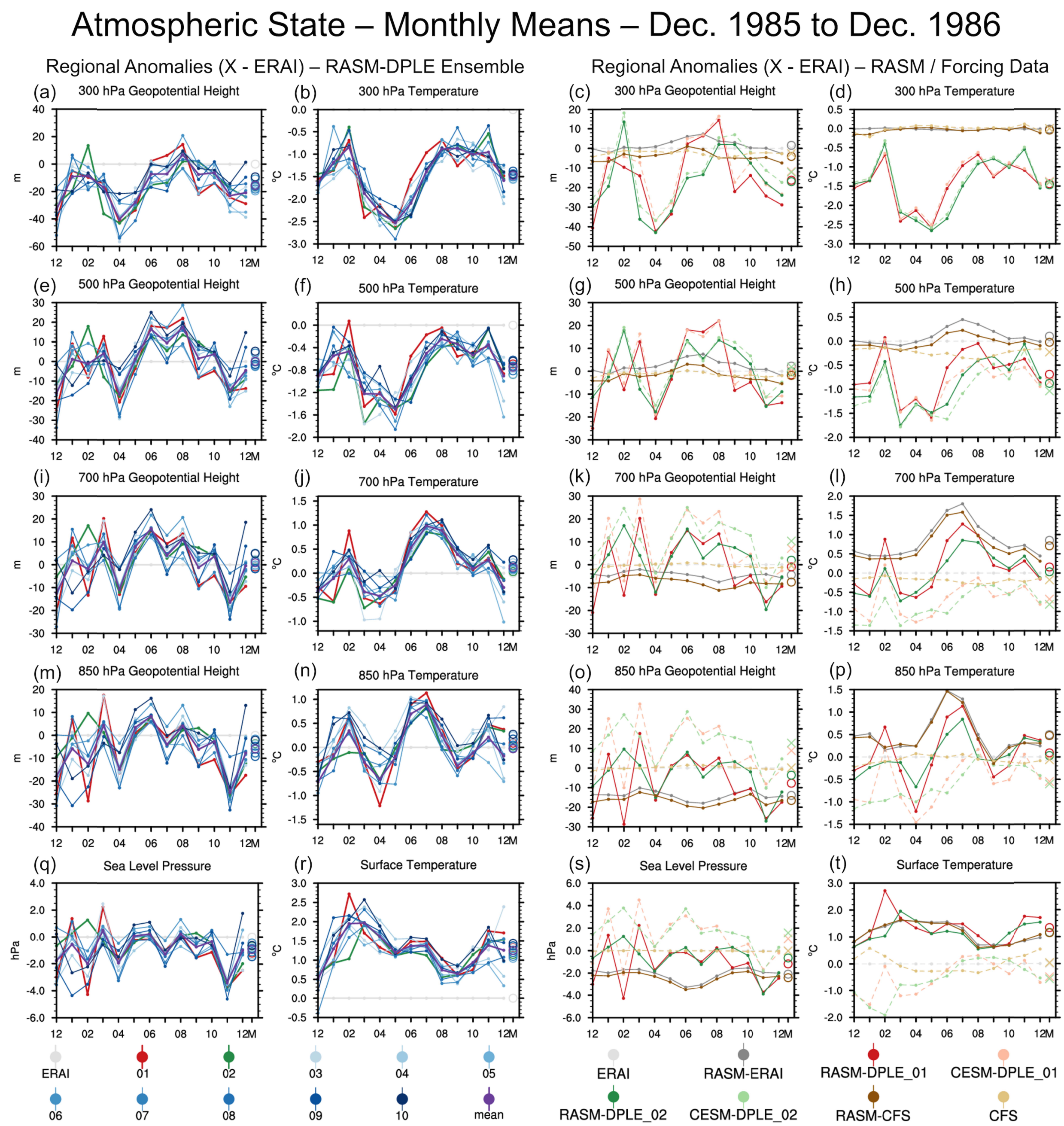

Figure 2. Monthly means of atmospheric state for the RASM domain spanning December 1985 to December 1986. The left two columns are for the 10 RASM-DPLE ensemble member simulations (01 - red, 02 - green, 03 to 10 shades of blue), the RASM-DPLE ensemble mean (purple), and the ERAI reanalysis (light gray). The right two columns are of the RASM simulations (solid lines) and the forcing data (dashed lines) for reanalyses (ERAI - grays, CFS - browns) and DPLE (01 - reds, 02 - greens). The open circles (Xs) are the 13-month means for the RASM simulations (forcing data). The means are plotted as anomalies in comparison to the ERAI reanalysis.

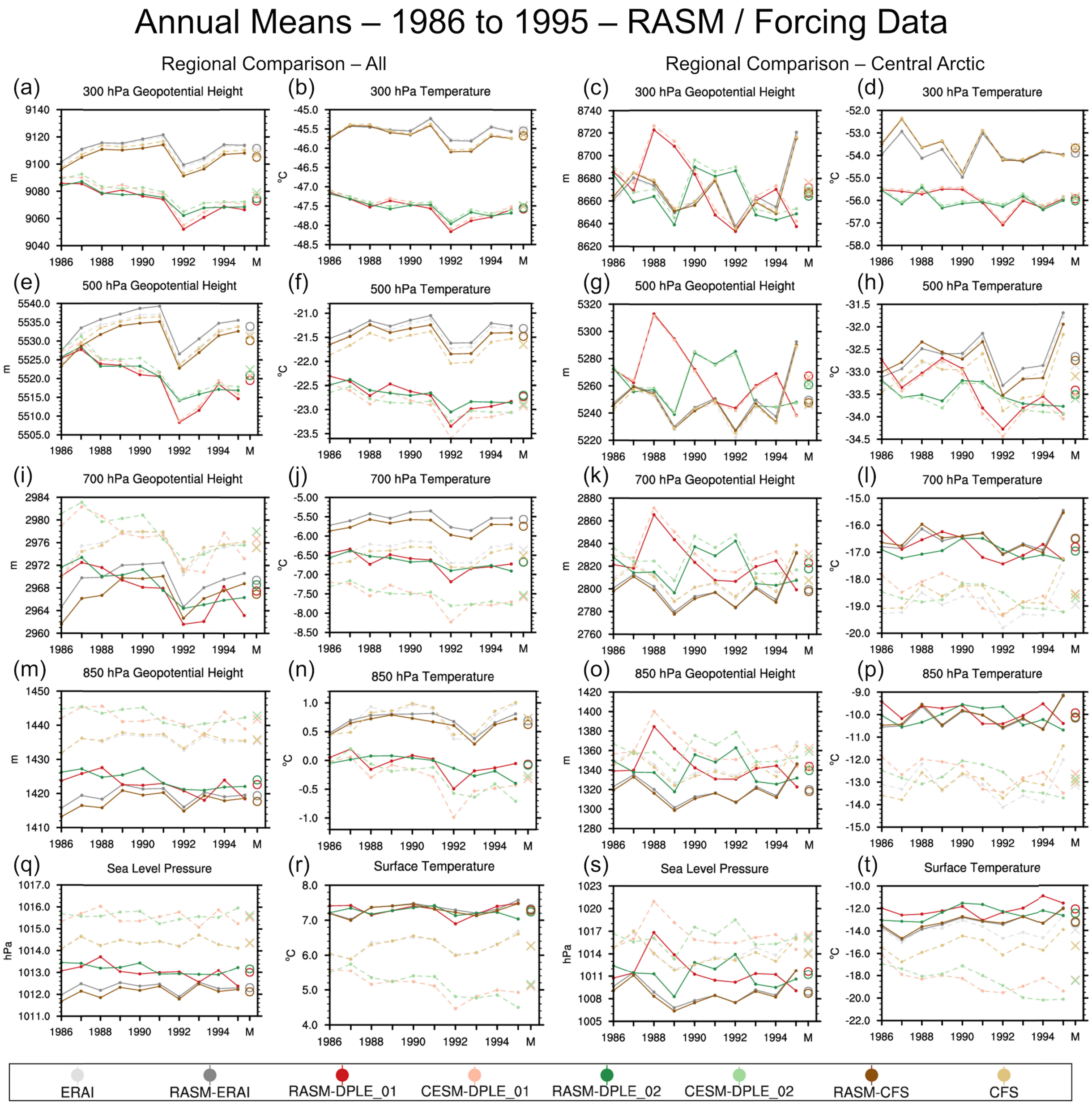

Figure 3. Annual means of atmospheric state spanning 1986 to 1995. The left two columns are the means for the RASM domain and the right two columns are the means for the Central Arctic analysis region. The plotted means are for the RASM simulations (solid lines) and the forcing data (dashed lines) for reanalyses (ERAI - grays, CFS - browns) and DPLE (01 - reds, 02 - greens). The open circles (Xs) are the 10-year means for the RASM simulations (forcing data).

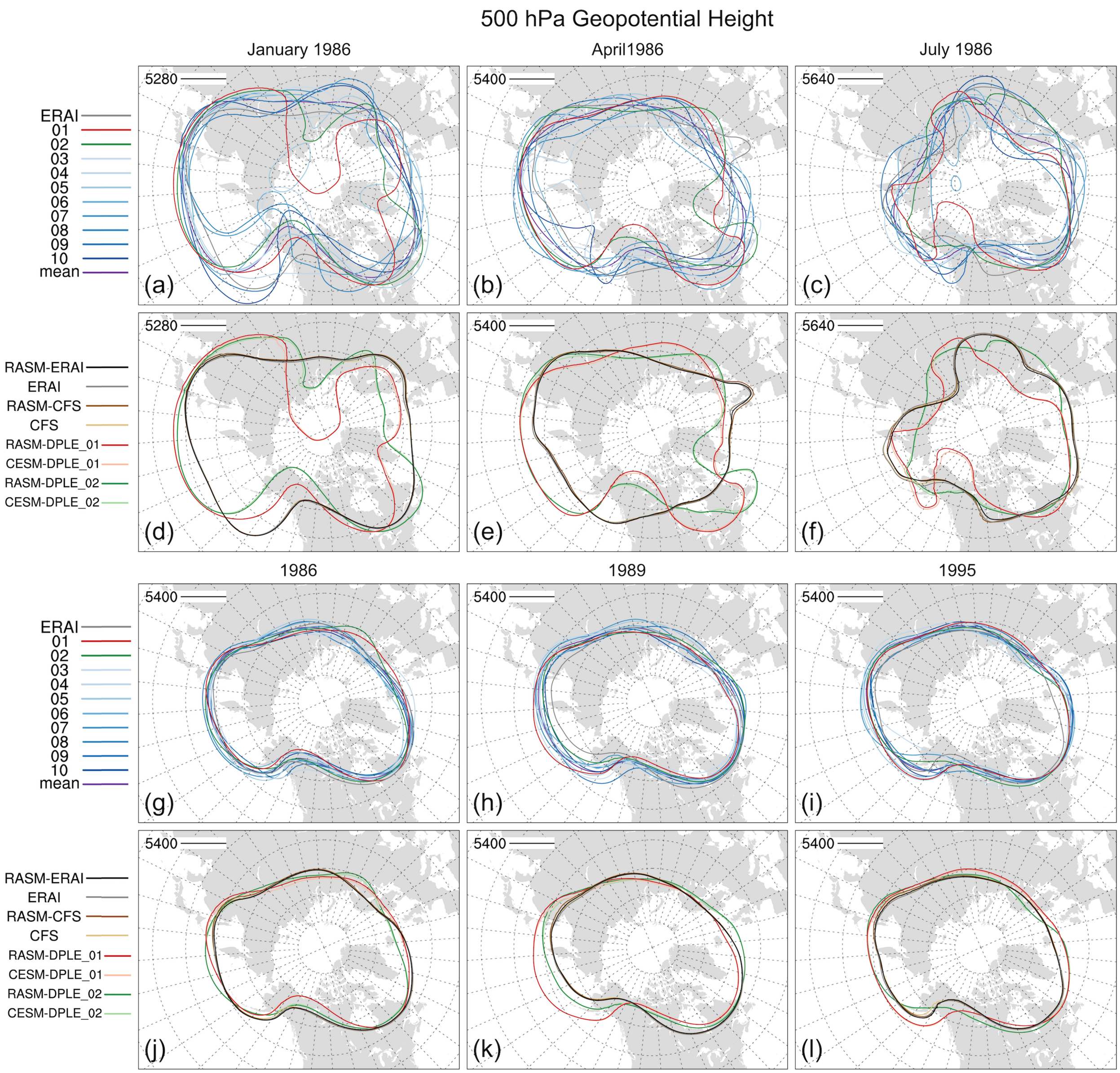

Figure 4. Spaghetti plot of a single 500 hPa geopotential height contour for the RASM domain. The top two rows are monthly means for January, April, and July 1986 and the bottom two rows are annual means for 1986, 1989, 1995. The contour is 5,400 m for all panels except January 1986 (a, d: 5,280 m) and July 1986 (c, f: 5,640 m). The first and third rows are for the 10 RASM-DPLE ensemble member simulations (01 - red, 02 - green, 03 to 10 shades of blue), the RASM-DPLE ensemble mean (purple), and the ERAI reanalysis (light gray). The second and fourth rows are of the RASM simulations (darker colors) and the forcing data (lighter colors) for reanalyses (ERAI - grays, CFS - browns) and DPLE (01 - reds, 02 - greens).

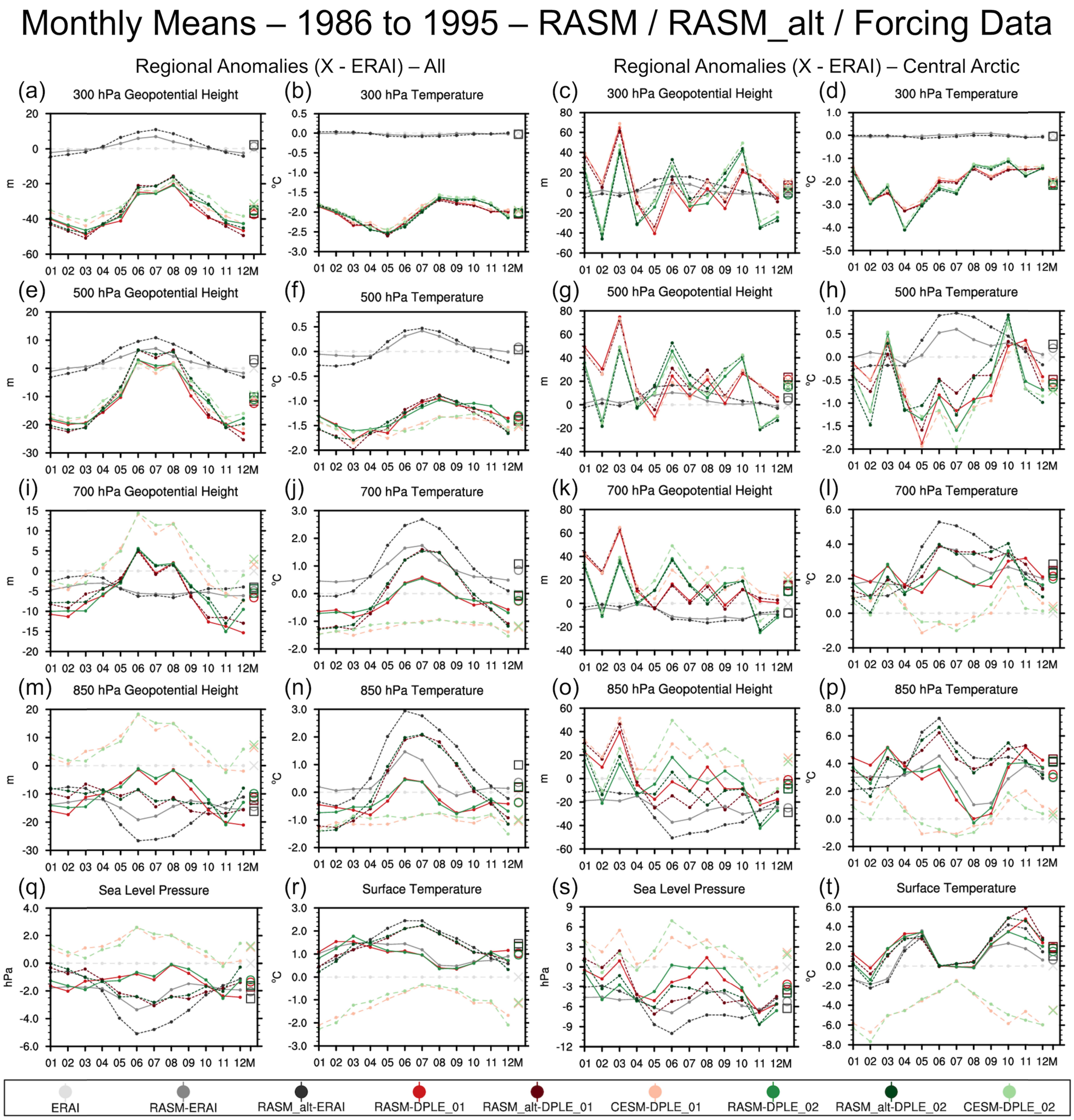

Figure 5. 10-year (1986-1995) monthly means indicating the annual cycle of the atmospheric state. The left two columns are the means for the RASM domain and the right two columns are the means for the Central Arctic analysis region. The plotted means are for the RASM_std simulations (solid lines), RASM_alt simulations (short-dashes, darker colors) and the forcing data (long dashes, lighter colors) for the ERAI reanalysis (grays) and DPLE (01 - reds, 02 - greens). The open circles, open squares, and Xs are the 10-year means for the RASM_std, RASM_alt simulations, and forcing data. The means are plotted as anomalies in comparison to the ERAI reanalysis.

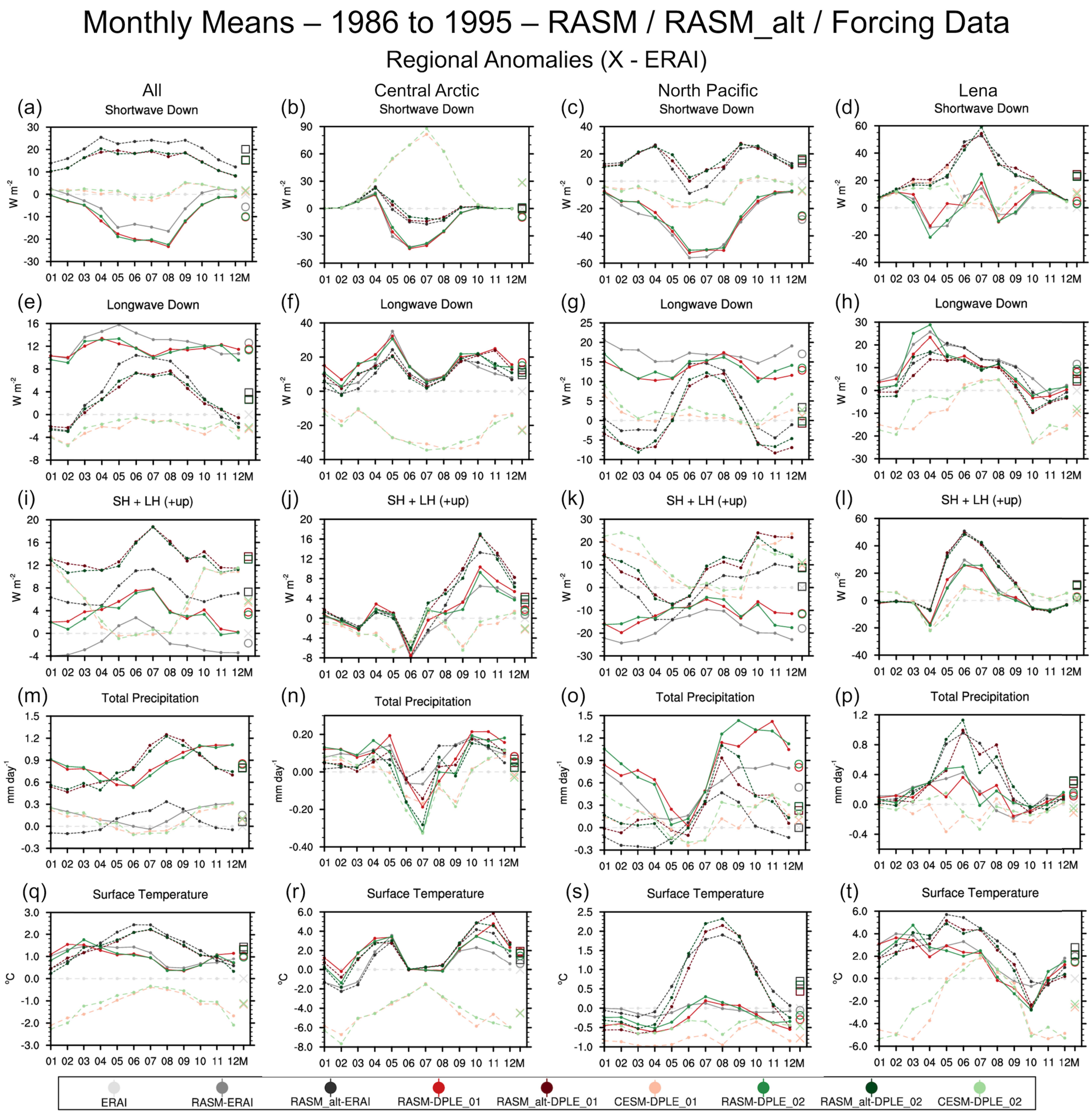

Figure 6. Same as Figure 5 except means of surface fluxes (SWD, LWD, SH+LH), total precipitation, and surface temperature with means for the RASM domain, Central Arctic, North Pacific, and Lena analysis regions in columns from left to right.

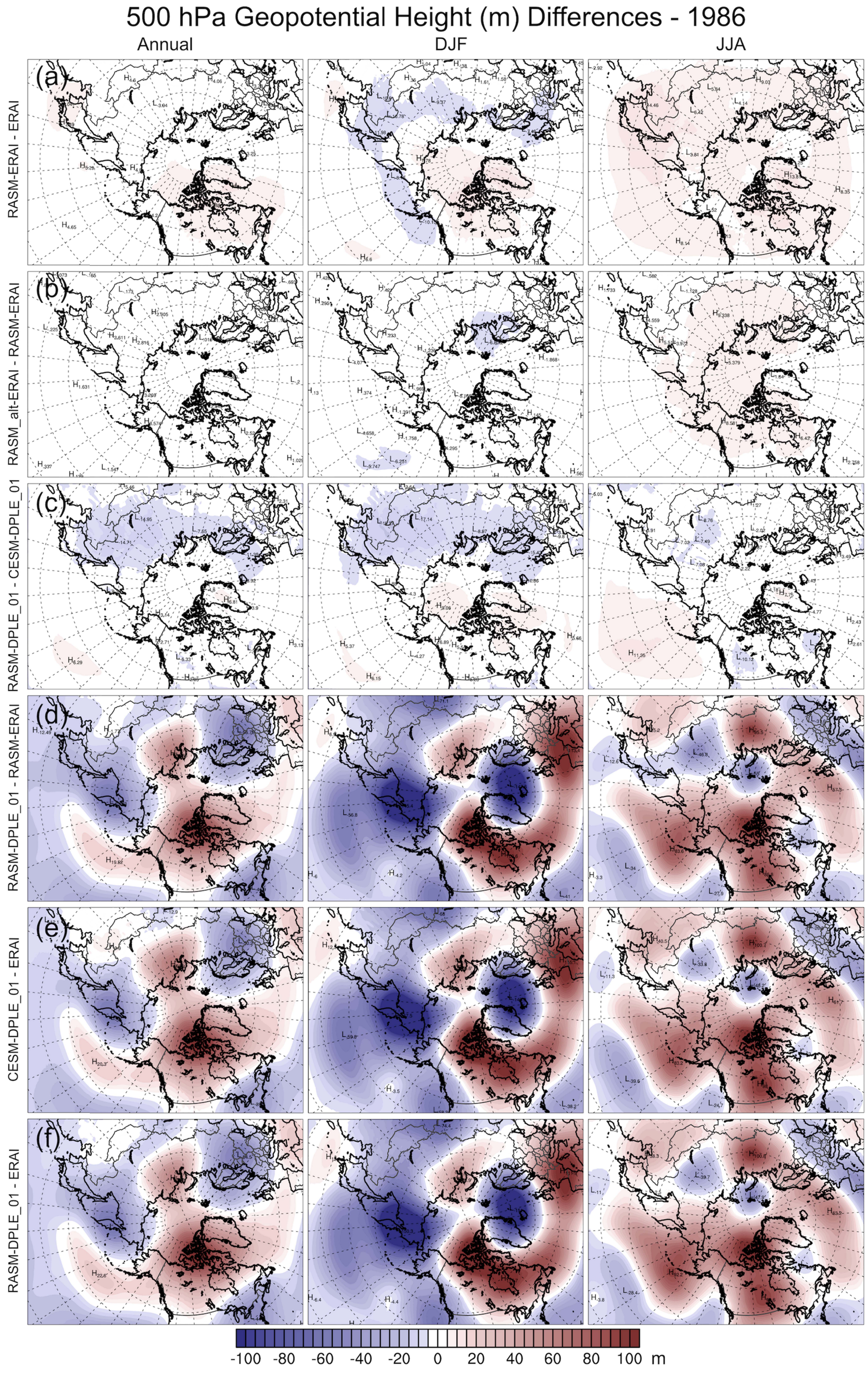

Figure 7. Spatial plots of differences in 500 hPa geopotential height (Z500) for 1986 across the RASM domain. The means are annual, December-January-February, and June-July-August in the columns from left to right. The differences are between RASM simulations / forcing data and other RASM simulations / forcing data as labeled along the left side of each row. The color bar indicates the contour of differences in mean Z500 with blues (negative) and reds (positive) differences.

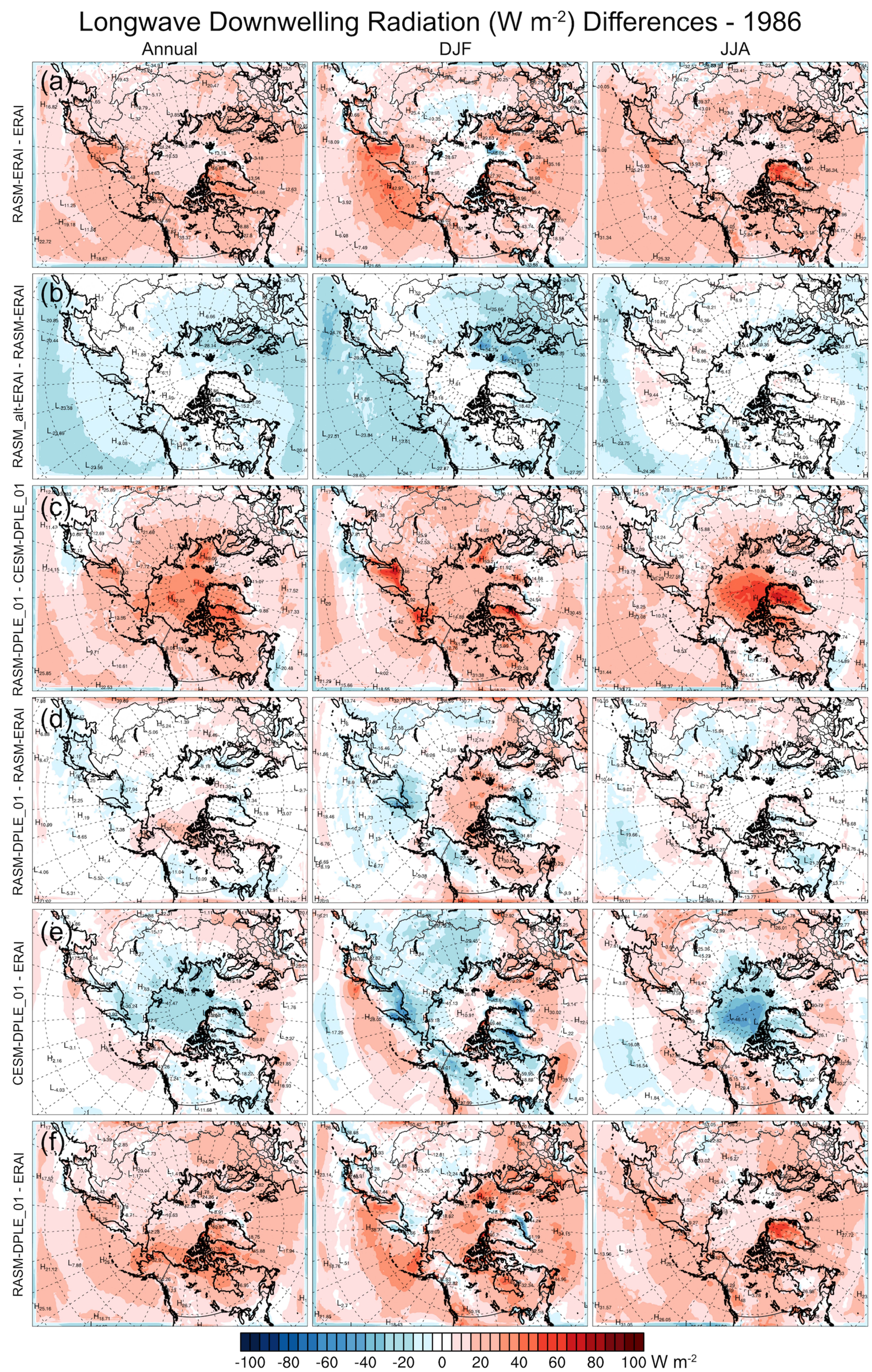

Figure 8. Same as Figure 7 except means of longwave downwelling radiation at the surface (LWD). The color bar indicates the contour of differences in mean LWD with blues (negative) and reds (positive) differences.

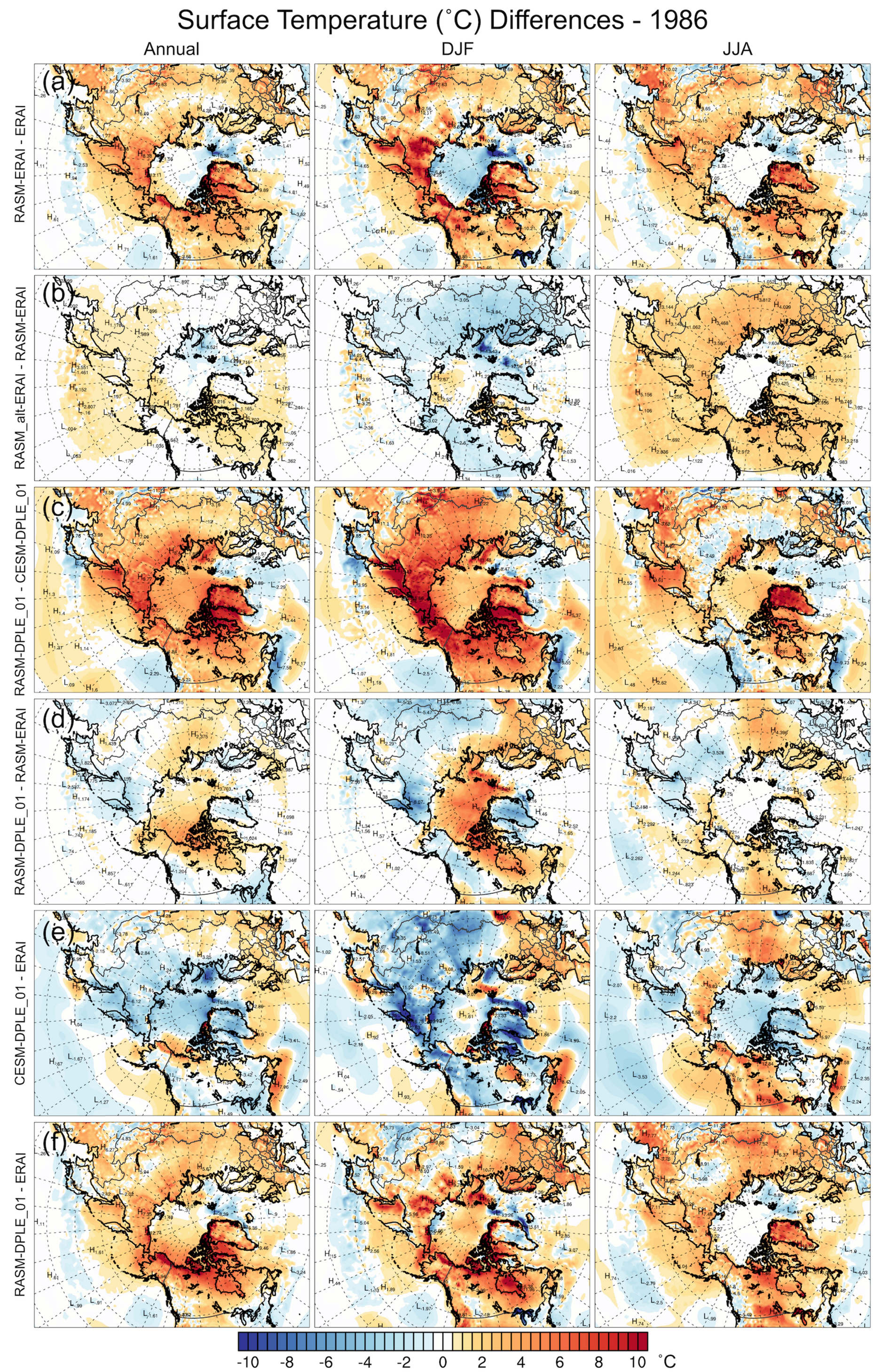

Figure 9. Same as Figure 7 except means of surface temperature (Tsfc). The color bar indicates the contour of differences in mean Tsfc with blues (negative) and oranges/reds (positive) differences.

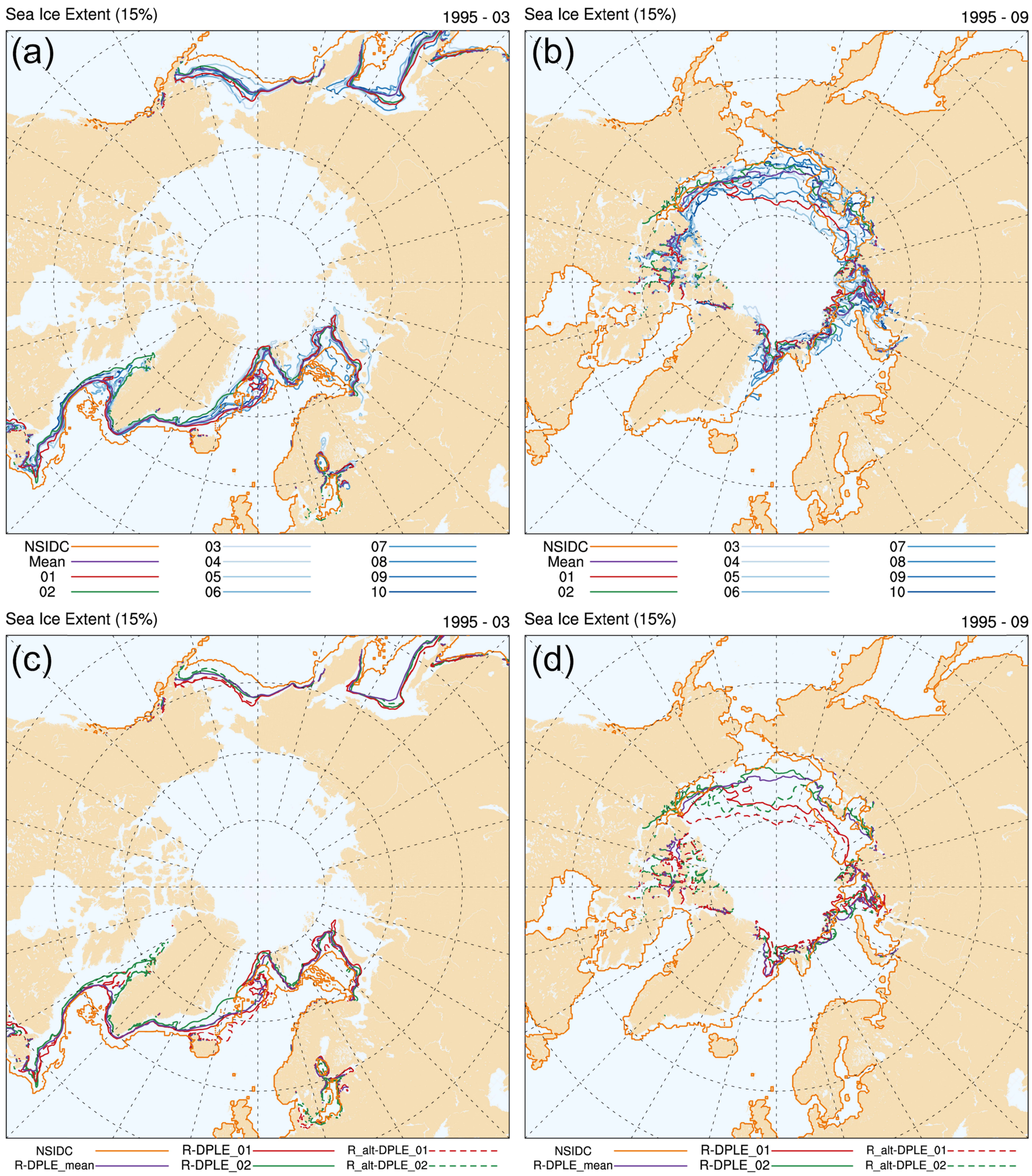

Figure 10. Spaghetti plot of sea ice extent, defined as 15% sea ice concentration, for March 1995 (left column) and September 1995 (right column) from the RASM simulations and the observations from the National Snow and Ice Data Center (NSIDC) as a reference. The top row is of the 10 RASM-DPLE ensemble member simulations (01 - red, 02 - green, 03 to 10 shades of blue), the RASM-DPLE ensemble mean (purple), and NSIDC (orange). The bottom row is of the RASM_std-DPLE 01 and 02 simulations (solid lines), RASM_alt-DPLE 01 and 02 simulations (dashed lines), the RASM_std-DPLE ensemble mean (purple) and the NSIDC observations (orange).

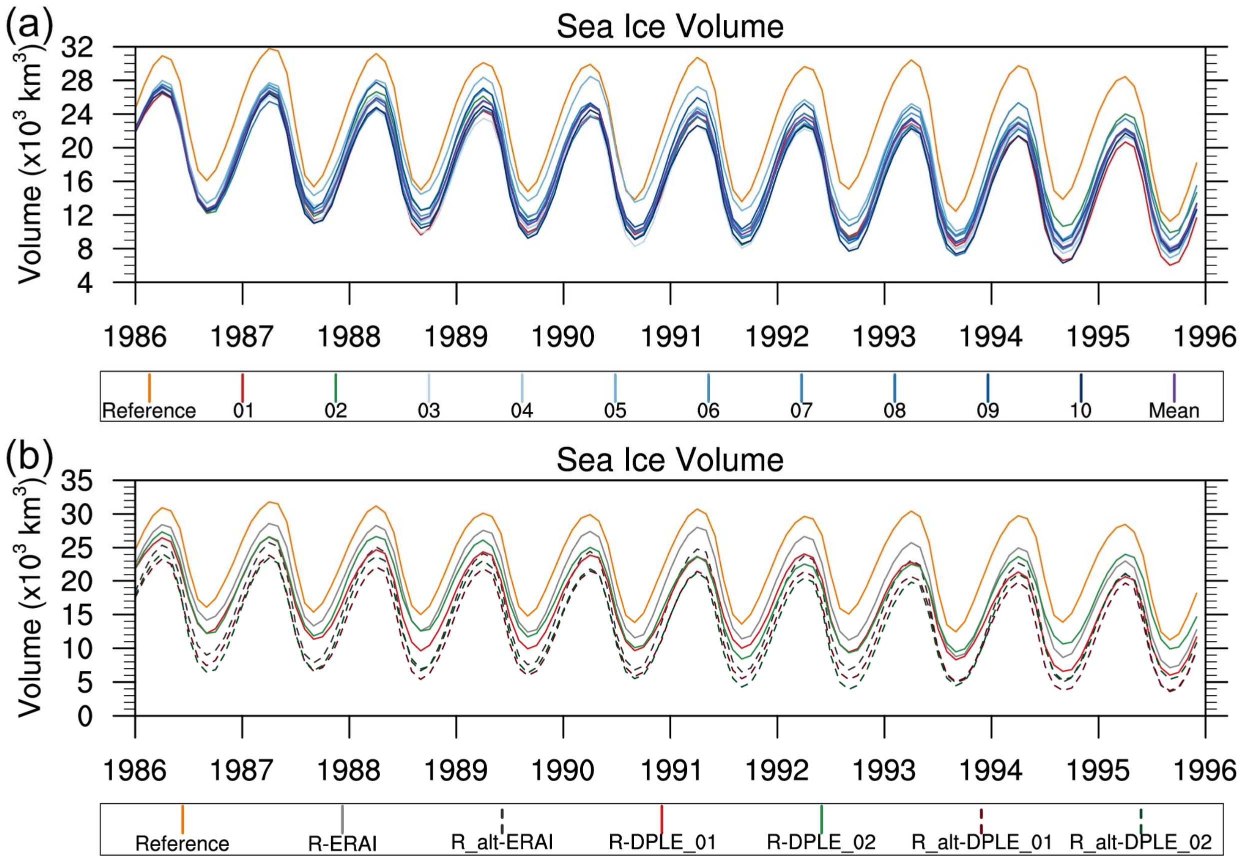

Figure 11. Time series plot of sea ice volume spanning 1986 to 1995. The top row is of the 10 RASM-DPLE ensemble member simulations (01 - red, 02 - green, 03 to 10 shades of blue), the RASM-DPLE ensemble mean (purple), and PIOMAS reference (orange). The bottom row is of RASM_std simulations (ERAI, 01, 02; solid lines), RASM_alt simulations (ERAI, 01, 02; dashed lines, darker colors), and PIOMAS reference (orange).

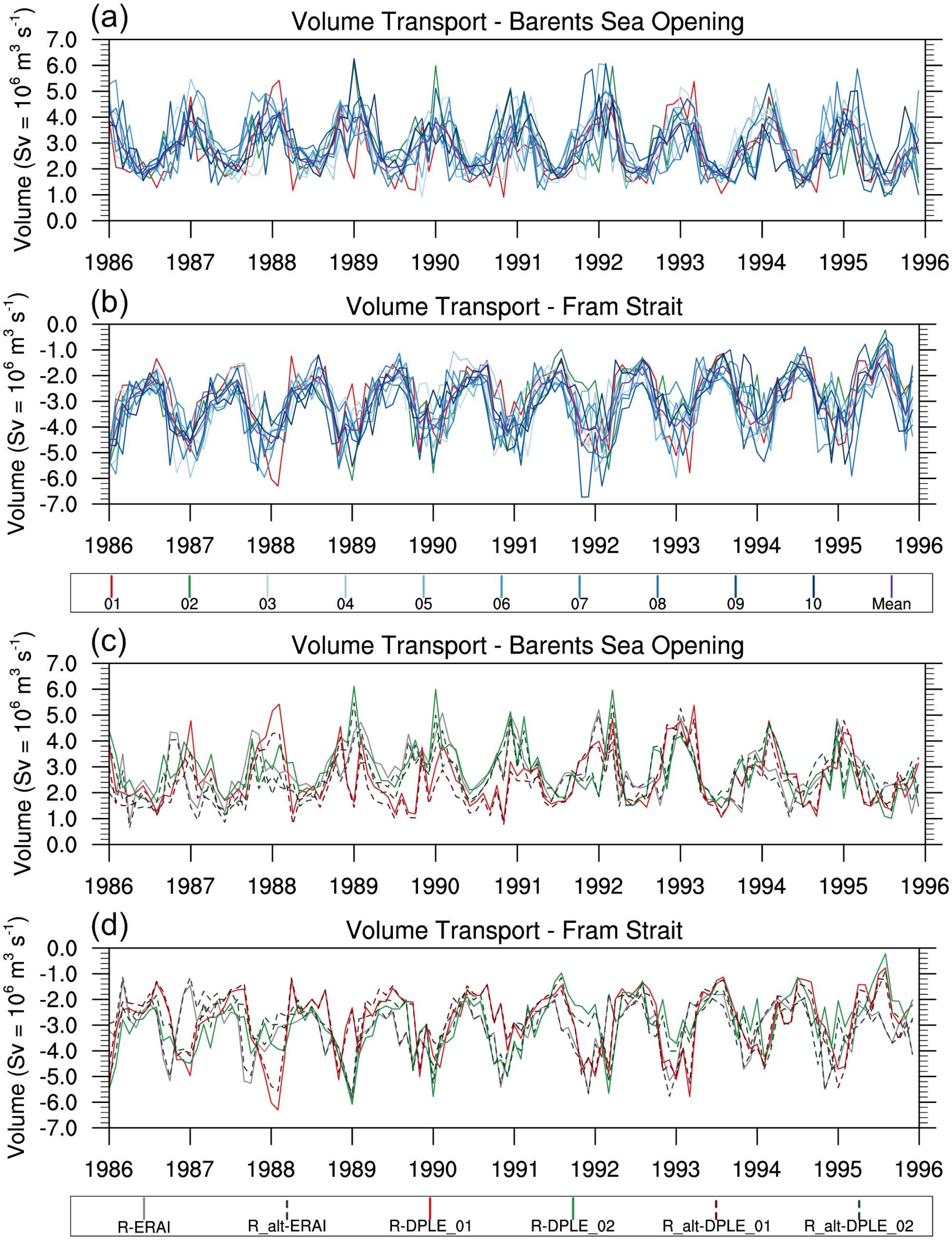

Figure 12. Time series plot of oceanic volume transport through the Barents Sea Opening (a, c) and the Fram Strait (b, d) gateways. The top two rows are of the 10 RASM-DPLE ensemble member simulations (01 - red, 02 - green, 03 to 10 shades of blue) and the RASM-DPLE ensemble mean (purple). The bottom two rows are of RASM_std simulations (ERAI, 01, 02; solid lines) and the RASM_alt simulations (ERAI, 01, 02; dashed lines, darker colors).